

RESEARCH EDITION · ALPHA 0.5 · 1 NOVEMBER 2026

xGEO
CORE

The simulation engine under xGEO: its physical models, the sources they rest on, how each is checked, and how to use it as an open-source tool

K. Williamson · xGEO project

BUILD	TESTS	COMPARISONS	ENGINE
Alpha 0.5	64	681 / 681 pass	Godot 4.7

681

of 681 comparisons within tolerance

64

automated tests against independent references

14

physical domains, from orbits to infrared

4

known simplifications, reported, not hidden

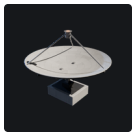
ABSTRACT

xGEO simulates a gray-zone confrontation in low Earth orbit. Its scenario, CLOSE PASS, is built on a real event: in October 2026 the Russian satellite Cosmos 2612 shadowed ICEYE-X36, a commercial radar-imaging satellite, at a few kilometres. The player commands WATCHMAN-1, a notional US inspector, and has to make Cosmos 2612 break off without contact, debris or open conflict, while keeping track of it with real ground radars. The craft start from public SGP4 element sets and fly under the Earth's gravity with its J2 flattening, the Sun and the Moon. This edition sets out every physical model the engine uses, with its equation, its source, how sure we can be of it, and which numbers are *design values* chosen for play. The engine's code is checked against JPL Horizons, hapsira, scipy, astropy, filterpy, ITU-R recommendations and published worked examples: 681 comparisons across 64 tests, all 681 within tolerance, and 4 further rows that report known simplifications. Section 11 lists what could not be verified.

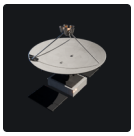
FIG. 1 WHAT THE GAME MODELS, AND WHERE TO READ ABOUT IT



ORBITS & EPHEMERIDES
§2–3 · SGP4, J2, Sun and Moon, Lambert



RADIO & DETECTION
§4 · ITU patterns, Friis, DF



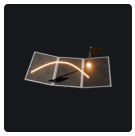
GROUND RADAR
§4.5 · five real sites



HEAT & SIGNATURES
§6 · energy balance, IR, shadow



TRACKING
§7 · unscented Kalman filter, custody



DOCTRINE & SCENARIO
§8–9 · the October 2026 incident

Every model is tested against an independent reference (§10). Click a box to jump to its section.

1 METHOD AND LABELS

The rule is that every number is either sourced or labelled. Each source claim carries one of four labels:

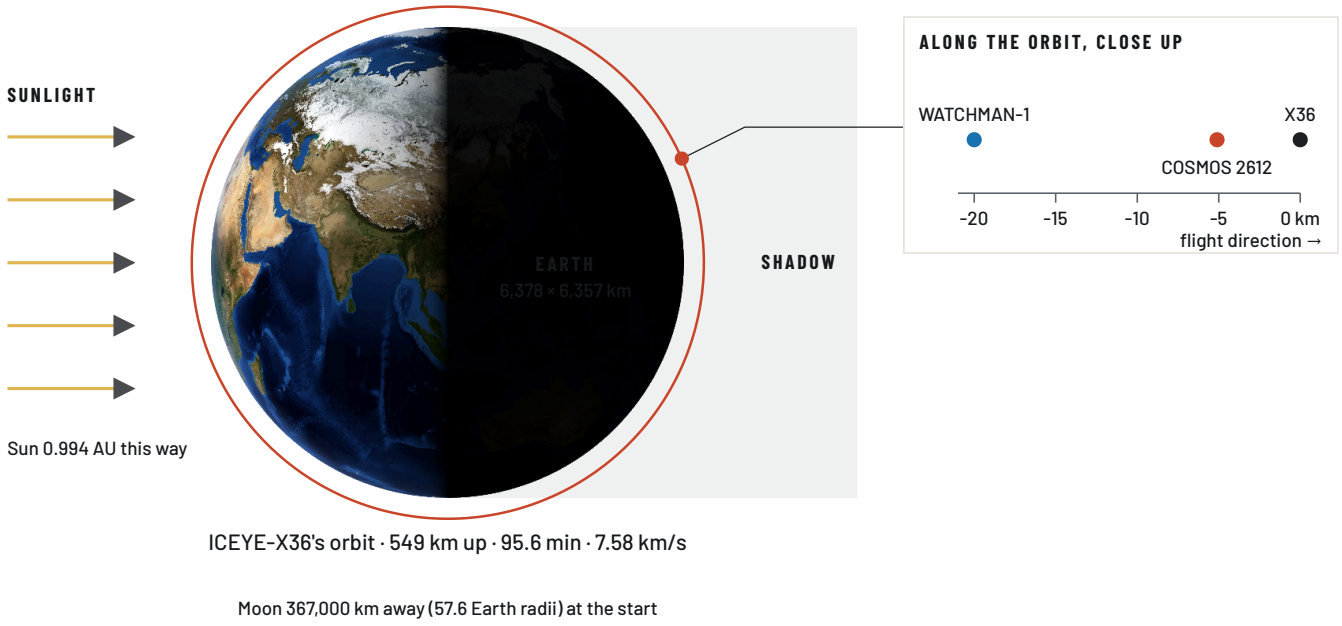
- V-TEXT The document was fetched and the passage read; the section, table or page is given.
- V-RECORD The work exists (publisher, DOI or official listing) but the passage was not read, because of a paywall or because it is a book. The equation used is the standard textbook form.
- UNVERIFIED Not confirmed. Treat it as unsourced.
- DERIVED Computed from verified inputs, with the method stated so it can be rerun.

Values chosen for play carry DESIGN VALUE. A design value is never presented as measured. Where possible, it is chosen inside a range that a source does support. The most important design values in CLOSE PASS are the inspector's plan (where it parks and for how long), the distances at which it gives way or leaves, the three hours of lost contact after which it withdraws (only with a Blue craft within 25 km of it), the tension costs, and the scenario's two days, against the weeks the real event took.

The game runs in Godot 4.7 (GDScript, with 64-bit arithmetic wherever precision matters). Its physics is tested by an external suite (§10), which reads the engine's own outputs. Python never reimplements the game in order to grade it.

2 FRAMES, TIME AND STARTING STATES

FIG. 2 THE SCENARIO, TO SCALE



The Earth and ICEYE-X36's orbit drawn to the same scale, with sunlight from the left and the shadow behind. At this scale the three craft sit on one point; the inset spreads them out along the orbit. Start positions from §2.2. Earth imagery: NASA Earth Observatory, Blue Marble Next Generation (Stöckli et al. 2005).

2.1 Reference frame and time

CLOSE PASS is centred on the Earth. Its axes are those of GCRF, the Earth-centred frame aligned with the ICRF: the Earth's mean equator and equinox of J2000 to within the frame bias of a few milliarcseconds. The Earth is an oblate body, 6,378.137 × 6,356.752 km (WGS 84), with GM = 398,600.4418 $km^3\ s^{-2}$ and J2 = 1.08262668×10^{-3} (EGM2008, as tabulated by Vallado[18]). The 3-D view uses a floating origin at the camera's focus, so positions keep their precision at any distance. The clock is UTC, starting at 21:00 UTC on 26 October 2026 and running two days. Leap seconds, TT − UTC and UT1 − UTC are ignored; §2.4 gives what that costs.

2.2 Starting states from public element sets

ICEYE-X36 (NORAD 59103, 2024-043F) starts on its real orbit. Its CelesTrak GP element set (epoch 26 October 2026, 21:06 UTC)[166] is propagated by SGP4 (Vallado et al. 2006[167]), whose output is in the TEME frame, and

then rotated into GCRF. The result is a near-circular orbit with semi-major axis 6,924.4 km: 549 km up, a period of 95.57 minutes and a speed of 7.584 km/s. SGP4 is used only for this starting state. From then on every craft is integrated under the force model of §3, which is how a real analyst would turn a catalogue orbit into a precise one.

Cosmos 2612 (NORAD 68762, 2026-083H) starts 5.1 km behind ICEYE-X36 and 140 m above it, where public element sets put it at 07:38 UTC on 18 October 2026 (KeepTrack's account of the rendezvous[168]). It is placed on the path that does not drift away along-track, which is how an inspector holds station. Blue starts with Cosmos 2612's catalogued orbit, about 200 m off its true one (a design value). WATCHMAN-1, the notional US inspector, starts 20 km behind ICEYE-X36.

CRAFT	ROLE	MASS	ΔV	SENSORS AND RADIO	SOURCE
ICEYE-X36	Target: commercial X-band SAR, operated by ICEYE US	90 kg	none modelled	3.25 m SAR antenna at 9.65 GHz	ESA Earth Online[160]; Gunter's Space Page[169]; GCAT[170]
Cosmos 2612	Red inspector, Russian Aerospace Forces	500 kg	≈ 90 m/s	0.1 m infrared camera; S-band command radio, 5 W into a 0.3 m dish	Mass, engine and radio notional; its observed moves, about 67 m/s from 30 Sep to 18 Oct, from public element sets[168]
WATCHMAN-1	Blue inspector (notional, after GSSAP)	675 kg	259 m/s	0.3 m telescope; 0.5 m receiving dish with a 2 m interferometer baseline	Mass within the 650–700 kg reported for GSSAP[150]; 4 × 22 N hydrazine at 2.2 km/s exhaust speed, 75 kg of propellant: design values

Table 1. The three craft. Values marked notional are DESIGN VALUES; GSSAP's sizes were never published.

2.3 The Sun and the Moon

The Sun's position comes from JPL's approximate Keplerian elements for the Earth–Moon barycentre (Standish & Williams[2], Table 1, valid 1800–2050), reversed to give the Sun as seen from the Earth: 0.9938 AU at the start. The barycentre lies about 4,700 km from the Earth's centre, which turns the Sun's direction by under 7 arcseconds. The Moon comes from the low-precision lunar series of Montenbruck & Gill[20] (§3.3.2, eqs. 3.47–3.48), good to a few arcminutes, about 500 km at the Moon's distance. It is 367,065 km away at the start. GM values come from DE440[3] (the Moon's 4,902.800118 $km^3\ s^{-2}$). Planets are added only beyond the Earth's sphere of influence, where their pull starts to matter.

2.4 The turning Earth and its ground sites

The ground radars of §4.5 and Cosmos 2612's handler near Moscow sit on the turning Earth. A site's position is rotated from the Earth-fixed frame into GCRF by Greenwich mean sidereal time (GMST 1982, Vallado[18] Alg. 15) and by IAU 1976 precession (Alg. 23), at the Earth's rate of 7.292115×10^{-5} rad/s. Nutation (under 20″), polar motion (under 0.5″) and UT1 − UTC (under 0.9 s) are omitted, so a site sits within about 1 km of where a full IERS reduction would put it. A radar measures what it sees from that point; a 1 km site error is about a thousandth of a typical range, and it is shared by every look from that site.

---

3 GRAVITY AND TRAJECTORY DESIGN

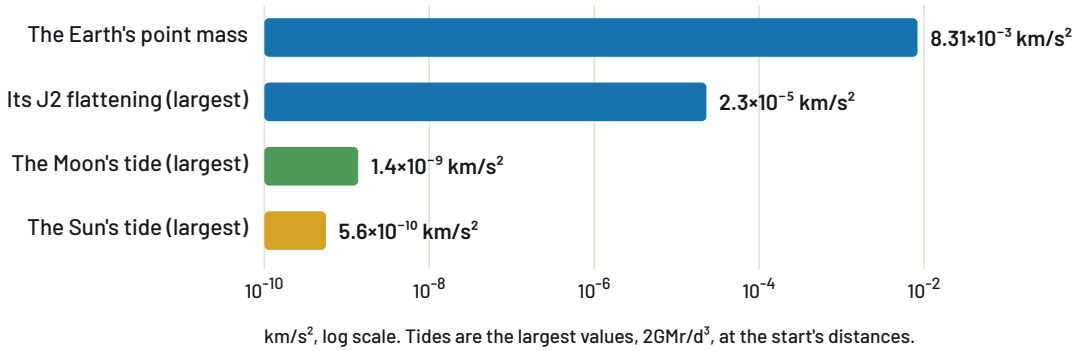
3.1 Force model and integration

The acceleration on a craft is the Earth's point mass, its J2 zonal term, and the Sun and the Moon as third bodies (direct minus indirect term; Montenbruck & Gill[20] §3.3, Cowell's method):

$$\mathbf{a} = -\mu\,\mathbf{r}/|\mathbf{r}|^3 + \mathbf{a}_{J2}(\mathbf{r}) + \Sigma_k\,\mu_k\left[\,(\mathbf{r}_k-\mathbf{r})/|\mathbf{r}_k-\mathbf{r}|^3 - \mathbf{r}_k/|\mathbf{r}_k|^3\,\right]$$

Integration is DOP853, the Dormand–Prince 8(5,3) pair with error control (Hairer, Nørsett & Wanner 1993), every step held to a relative 10^{-12}, so steps lengthen on quiet arcs and shorten near a close pass, with no step rule to tune. Against scipy's DOP853 at 10^{-13} on the same forces, the engine stays within 2.8 mm over a day, and within 0.13 m over a 20-day J2 arc. The classical fourth-order Runge–Kutta step stays in the code for tests. There is no atmospheric drag (§11). The same engine, run on its own, centres the world on Jupiter with the four Galilean moons as its third bodies; the external suite of §10 checks that world against JPL Horizons.

FIG. 3 WHAT PULLS ON A SATELLITE AT 549 KM



The force model of §3.1 at ICEYE-X36's radius. The Sun and the Moon are a millionth of J2, but over two days they move a craft by tens of metres, which is the scale of a close approach.

For the Earth, two checks run in Godot on every change. ICEYE-X36's orbital node turns 1.0395° per day, against 1.0400° from J2's first-order secular rate (Vallado eqs. 9-41/42). And a craft placed on the no-drift path beside it stays within 779 m of it over a whole orbit, which shows that the starting states and the forces agree.

3.2 Two-body tools

Kepler propagation uses universal variables (Curtis[17] Alg. 3.3–3.4), with Danby's starter near e = 1 and Vallado's starter for long hyperbolic coasts (Vallado[18] Alg. 8). Lambert's problem is solved by Izzo's method (Izzo 2015[23]), including multi-revolution transfers. Across 111 test transfers it agrees with hapsira's Izzo solver to 7.3e-15, and it reproduces Curtis Example 5.2. An earlier build used Curtis Alg. 5.2; a loss of precision in its Stumpff function as $z \to 4\pi^2$ made every transfer over 180° fail, which was one reason for the change.

3.3 Refining under full gravity

Over a 3-hour coast in low orbit, J2 alone moves a craft by kilometres, so a two-body Lambert solution misses a target only a few kilometres away. Every planned burn is therefore refined by differential-correction shooting through the full-gravity coast (Vallado[18]; single shooting as set out in NASA/TP-20220014814 §5.2.1). Newton's method starts from a two-body Jacobian and updates it with Broyden's method[24]. A 3-hour move by WATCHMAN-1 from 20 km behind ICEYE-X36 to beside it is planned at 0.74 m/s and flies at 0.75 m/s.

3.4 The planner

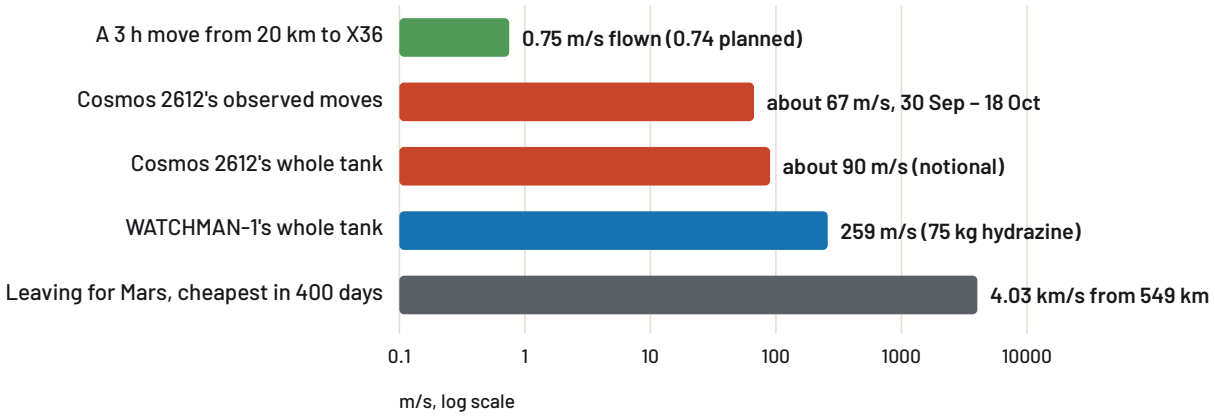
The planner shows a porkchop plot: departure wait against time of flight, each cell a refined transfer coloured by the Δv to go and the Δv to match on arrival. Its grid steps are design values. Close to a target, the

planner also offers station-keeping: holding a point a set distance ahead, behind, above or beside the target. A point 1 km out of ICEYE-X36's plane is held at 1.00 km.

3.5 Leaving Earth orbit

Where a scenario allows it, the planner plans between planets with patched conics (Curtis ch. 8; Vallado ch. 12). A heliocentric Lambert arc runs between the planets; the escape burn is fitted so its hyperbola leaves from the ship's actual position; and the plan is refined under full gravity. Spheres of influence follow Laplace, $r = a(m/M)^{2/5}$ (Curtis §8.4). From ICEYE-X36's orbit, the cheapest departure for Mars in the 400 days after the start costs 4.03 km/s. WATCHMAN-1 carries 259 m/s, Cosmos 2612 about 90. Interplanetary flight is switched off in CLOSE PASS, and these figures show it would be out of reach anyway.

FIG. 4 FUEL AGAINST WHAT THINGS COST



Δv from §3.3–3.5 and §9. Close-in moves are cheap; WATCHMAN-1 can make hundreds of them. Leaving Earth orbit is out of reach of every craft here, which is real physics, not a game limit.

4 RADIO AND RADAR: ANTENNAS, LINKS AND DETECTION

4.1 Antenna gain and patterns

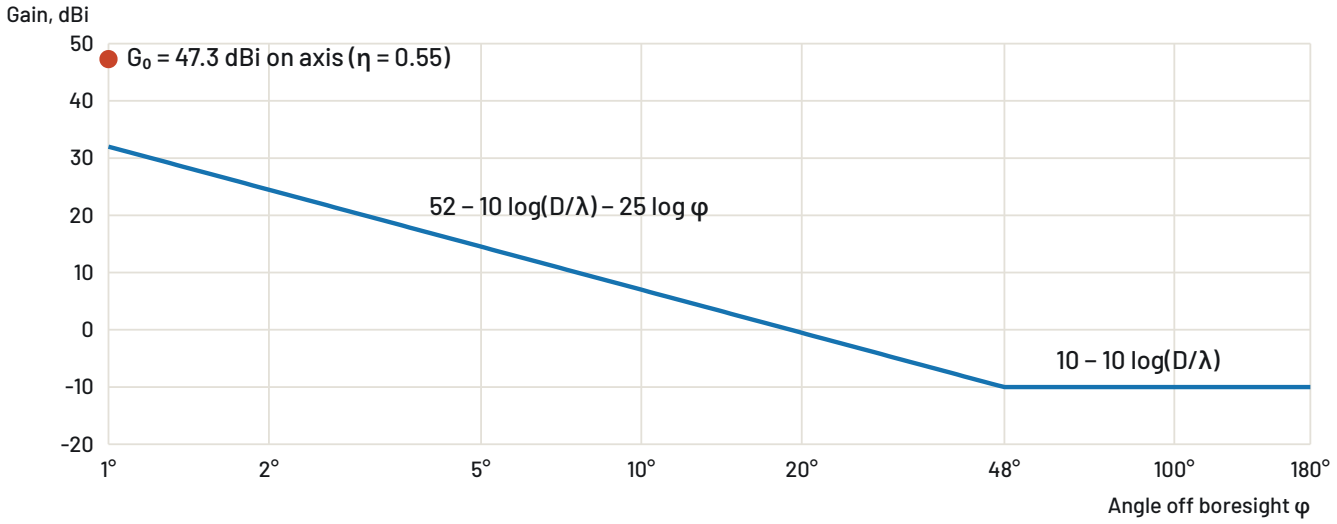
The peak gain of a dish of diameter D at wavelength λ is $G_0 = \eta(\pi D/\lambda)^2$, with $\eta = 0.55$ throughout. That is 1.24 dB conservative against the DSN 34 m antenna at X band (68.24 dBi at 8425 MHz, DSN 810-005 Module 104 Rev. O Table 8[39]). The beamwidth is about $70\lambda/D$ degrees (NAWCWD TP 8347 §3-1[54]; ITU-R SA.509-3 §1.3[33]) V-TEXT.

Off-axis gain follows the ITU reference envelopes: SA.509-3 for large dishes (D/λ ≥ 100), and S.465-5 Note 4 for small ones[34]:

$$G(\phi) = 52 - 10\log(D/\lambda) - 25\log\phi \quad \text{dBi}, \quad 100\lambda/D \le \phi < 48^\circ$$
$$G(\phi) = 10 - 10\log(D/\lambda) \quad \text{dBi}, \quad 48^\circ \le \phi \le 180^\circ$$

These are envelopes of sidelobe peaks, used in interference coordination, so they are conservative for a well-designed antenna. Note 2 of S.465 warns against using them below D/λ = 50, and every Red dish in the game is that small. They are still the most credible public pattern. Every emitter points. In CLOSE PASS, Cosmos 2612's command radio aims its 0.3 m dish at its handler near Moscow, and WATCHMAN-1 listens through a 0.5 m dish of its own. Warships and buoys in the engine's other world listen through four-face arrays that form beams in all directions (after the TDRS S-band multiple-access array, NASA TM-105422), with gain equal to the face's peak plus 10 log cos(scan).

FIG. 5 REFERENCE ANTENNA ENVELOPE



ITU-R SA.509-3 sidelobe envelope drawn for an illustrative dish 100 wavelengths across. It is an envelope of sidelobe peaks, so it is conservative for a well-designed antenna.

4.2 Link budget and noise

$$P_r = P_t\, G_t(\theta_e)\, G_r(\theta_r)\, (\lambda / 4\pi R)^2 \qquad \text{(Friis 1946)}$$
$$N = k\, T_s\, B$$

Free-space loss is the exact 20 log(4πR/λ) of ITU-R P.525-4 eq. (3). The practical eq. (4) rounds its constant to 32.4 dB (exactly 32.448 dB), so the game differs from eq. (4) by 0.048 dB.

4.3 Detection of unknown bursts

Listeners don't know a burst's waveform, so they detect it with an energy (radiometer) detector (Urkowitz 1967[51]). The integrated SNR grows as $\sqrt{(B\tau)}$. The chance of detection is:

$$P_d = Q\left(\left(Q^{-1}(P_{fa}) - d\right) / \sqrt{(1 + 2s)} \right), \quad P_{fa} = 10^{-6}$$

The false-alarm rate is a DESIGN VALUE. This expression matches the exact chi-square distributions to 0.01 for $n \geq 10^5$ samples, and even odds come at 6.8 dB. Spreading a signal over a wider band costs an eavesdropper's energy detector $\sqrt{(B_{old}/B_{new})}$ in SNR at fixed power (the radiometer equation; Urkowitz 1967[51]). ITU-R SM.1055[38] §1 notes that spread signals are noise-like and not readily detected.

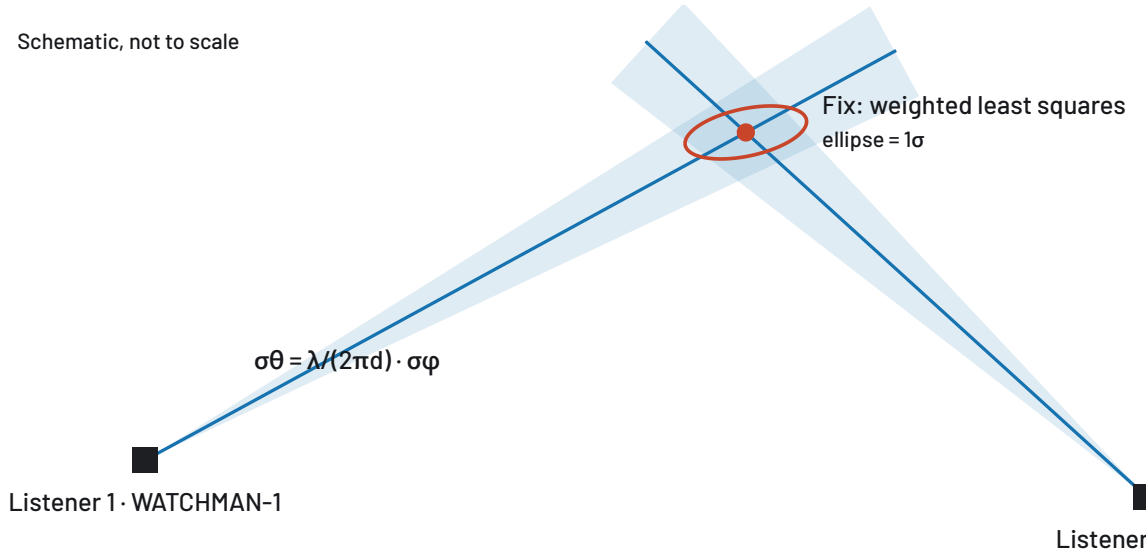
4.4 Direction finding and identification

A two-element interferometer measures a bearing with

$$\sigma_\theta = \lambda/(2\pi d) \cdot \sigma_\phi, \quad \sigma_\phi^2 = (1 + 2s) / (2B\tau\, s^2)$$

This is the cross-correlation phase error for a noise-like signal. It follows from the Knapp & Carter (1976) Cramér–Rao bound in terms of coherence, $\gamma^2 = s^2/(1 + s)^2$, in the narrowband limit; it is checked by a Monte Carlo of a two-element correlator to 3%. A 20 µrad floor is a DESIGN VALUE. Bearings from separated listeners are crossed by weighted least squares. Identification compares a recording's modulation and symbol rate against a threat library above a minimum SNR, a design-value gate. Specific-emitter identification is real: it recognises a device by imperfections in its analog circuitry (Danev et al.[78]).

FIG. 6 DIRECTION FINDING



Two listeners (in CLOSE PASS, WATCHMAN-1's two receivers 2 m apart, or two craft) each take a bearing with its own error wedge. The fix is their weighted least-squares crossing; the farther apart the listeners, the tighter the ellipse. Schematic.

4.5 Ground radar

Five real radar sites track the three craft. Each look returns range, azimuth and elevation, each with Gaussian noise, every 10 seconds while the craft is above the site's elevation mask and inside its reach. The site's position follows the turning Earth (§2.4): PFISR, at 65.1° N, moves 704 km in an hour, at 0.1962 km/s: the Earth's rate times its 2,690 km distance from the polar axis on WGS 84 gives 0.1961 km/s (DERIVED). Range noise is published for three of the sites; angle noise and masks are notional.

SITE	OPERATOR	RANGE Σ	ANGLE Σ	MASK	REACH	SOURCE
PFISR, Poker Flat, Alaska	SRI International / NSF; LeoLabs	14 m	0.05°	45°	3,000 km	Site and range noise: Nicolls et al. 2017[171], Table 1
Midland Space Radar, Texas	LeoLabs	14 m	0.1°	30°	3,000 km	Site and range noise: Nicolls et al. 2017[171]
Kiwi Space Radar, New Zealand	LeoLabs	17 m	0.02°	40°	1,500 km	Site, range noise and reach: Stevenson et al. 2020[172]
Arizona Space Radar	LeoLabs	15 m	0.05°	20°	3,000 km	Site: FCC experimental licence WO2XME[173]; noise notional
Space Fence, Kwajalein	U.S. Space Force, 20 SPCS	15 m	0.02°	20°	3,000 km	Notional: not published

Table 2. Ground radar in CLOSE PASS. Angle noise, masks and Space Fence's figures are DESIGN VALUES.

A radar at a site differs from one on a ship in two ways that matter here. It sees a craft only for a few minutes per pass, so custody between passes rests on the filter's prediction (§7). And its range noise, tens of metres, is far smaller than its angle noise at 1,000 km (0.05° is 870 m across the line of sight), so a single pass fixes how far away a craft is much better than where across the sky.

---

5 ELECTROMAGNETIC ATTACK AND TENSION

The engine models jamming, spoofing, dazzling, high-power microwaves, cyber takeover and kinetic kills, and its other world uses them all. CLOSE PASS gives Blue none of them: WATCHMAN-1's only lever is its presence. The models are kept here because they are part of the engine, and because a scenario that adds a jammer would rely on them.

5.1 The jamming equation

Jamming a command uplink means being louder, at the victim's receiver, than its handler. Both paths are one-way, so the equation is Friis applied twice. This is the communications form of NAWCWD TP 8347 §4-9 V-TEXT, and Adamy's EW 101[75] gives it in dB form:

$$J = P_j + G_j(\text{aim error}) + G_v(\theta_j) - L_j$$

$$S = P_u + G_u + G_v(0) - L_s$$

$$J/S = J - S - 10\log(B_j/B_v) \quad \text{dB}$$

$G_v(\theta_j)$ is the victim's gain toward the jammer, at angle θ_j off its line to the handler, so geometry matters: a jammer near the handler's line faces the victim's main beam. The aim term means a loose track costs beam-pointing gain. Before the signal is identified, a jammer must spread its power across the whole allocation (barrage); once identified, it can put it all in the channel (spot). How much J/S breaks a link has no universal number. NAWCWD §4-7 (p. 4-7.3) says plainly that effectiveness "is not a direct mathematical function of J/S" V-TEXT. The engine requires +6 dB, a DESIGN VALUE inside the 0–10 dB band typical for FEC-coded BPSK.

5.2 Other effects

EFFECT	MODEL	SOURCE / STATUS
Spoof (FAKE)	False ranging tones capture the target's ranging loop at J/S ≥ 0 dB, inducing a drift	Loop capture at 0 dB and a drift of 900 km/h are design values
Dazzle	Spot radius $R\sqrt{((1.22\lambda/D)^2 + j^2)}$ at 1.06 µm, 2 m aperture, 0.2 µrad jitter; 10 W/m² at the aperture	Airy disc 1.22λ/D (Hecht); jitter added in quadrature (engineering approximation); 10 W/m² is an engineering estimate allowing for an OD-6 filter
HPM (PULSE)	Far field $E = \sqrt{(30PG)}/R$ from a 1 GW-peak X-band source; front-door damage at 100 V/m	$E = \sqrt{(30PG)}/R$ (Balanis; ITU-R P.525-4 eq. 1); 100 V/m is a DESIGN VALUE (engineering estimate); GW-class backward-wave oscillators (Benford et al. 2016)
Cyber (TAKE)	Takeover after recording enough command traffic	Abstracted. Real command links are encrypted, and this is stated as fiction
Kinetic kill	$P_k = \text{rel}\cdot(1 - e^{-r^2/2\sigma^2})$, from divert reach against track uncertainty	Rayleigh. Breakup by the NASA standard breakup model (below). The 1,200 catalogued pieces are a DESIGN VALUE set below FY-1C (2007; 3,442 catalogued[138]) and Cosmos 1408 (2021)

A kill breaks the wreck up by the NASA standard breakup model (Johnson et al. 2001[131], as given in Frey & Colombo 2021 App. B[135]). An impact is catastrophic above 40 J/g, and $N(\geq L_c) = 0.1\ M^{0.75}\ L_c^{-1.71}$ fragments are drawn. Each fragment's area-to-mass ratio $\chi = \log_{10}(A/M)$ follows App. B: the bimodal spacecraft law above 11 cm, the small-object law below 8 cm, and a linear blend in $\log L_c$ between 8 and 11 cm. Its speed follows $\log_{10} \Delta v \sim N(0.9\chi + 2.9, 0.4)$, Δv in m/s.

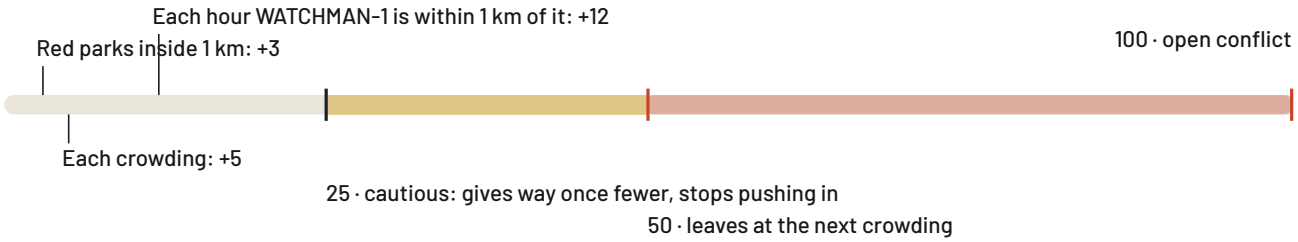
5.3 Escalation in the engine

Each effect carries an escalation cost, a design value: jamming 2 per hour, radar 1 per hour, spoofing 4, dazzling 8, cyber 10, high-power microwave 15, and a kinetic kill 45. Doctrine provides no escalation ladder (§8).

5.4 Tension in CLOSE PASS

CLOSE PASS has its own meter, because its only acts are approaches. Tension rises by 3 when Cosmos 2612 parks inside ICEYE-X36's 1 km keep-out, by 5 each time WATCHMAN-1 crowds it into giving way, and by 12 for every hour WATCHMAN-1 spends within 1 km of it. At 25, Cosmos 2612 turns cautious: it gives way once fewer before leaving, and it stops pushing in. At 50 it leaves at the next crowding. At 100 the confrontation has become open conflict and the scenario is lost. Every value is a DESIGN VALUE.

FIG. 7 TENSION IN CLOSE PASS



The tension meter of §5.4. Every value is a DESIGN VALUE. Doctrine gives no ladder (§8); this one rewards pressure that stops short of contact.

6 HEAT, INFRARED AND VISIBLE SIGNATURES

6.1 Energy balance

Each craft has a skin and, if it carries a reactor, radiators. Skin temperature follows a single-node balance with heat capacity (Gilmore[103]):

$$C\,\frac{dT}{dt} = P_{leak} + \alpha\, S\, f\, A/4 - \varepsilon\,\sigma\, T^4\, A, \qquad C = 897\ \mathrm{J\,kg^{-1}\,K^{-1}} \times 0.25 \times m_{dry}$$

$S = 1{,}361\ \mathrm{W\,m^{-2}}$ at 1 AU (Kopp & Lean 2011[109]), scaled by the inverse square of the Sun's distance, and f is the sunlit share (§6.4). The heat capacity is aluminium's at 298 K, 24.21 J $\mathrm{mol^{-1}\,K^{-1}}$ or 897 J $\mathrm{kg^{-1}\,K^{-1}}$ (NIST-JANAF, NIST Chemistry WebBook[105]); Incropera[104] Table A.1 gives 903 J $\mathrm{kg^{-1}\,K^{-1}}$ at 300 K, 0.7% more. The 25% skin fraction is a DESIGN VALUE. WATCHMAN-1's skin has a time constant of about 1.5 hours (DERIVED: $C = 897 \times 0.25 \times 600\ \mathrm{kg} = 134{,}550\ \mathrm{J/K}$ against $4\varepsilon\sigma T^3 A \approx 25\ \mathrm{W/K}$), so it cools noticeably during each pass through the Earth's shadow, which lasts up to about 36 minutes at 549 km. The Earth's own reflected sunlight (albedo

0.367) and its infrared glow (254 K as a black body) are not yet added to the heat balance (§11). Absorptance and emittance come from NASA RP-1121 (Henninger 1984[95]).

The engine also models reactor radiators, after the 100 kWe Brayton plant of NASA Glenn's JIMO study (Mason 2003[96]; Siamidis 2005[98]), as two-sided Lambertian plates, $I(\theta) = \varepsilon\sigma T^4 A \cos\theta/\pi$. No craft in CLOSE PASS carries a reactor.

6.2 Going dark

A reactor ship can stop radiating for a while by storing its heat in water it vents (2.5 MJ/kg) or ice it melts (333 kJ/kg, Leimkuehler 2011[102]). This is part of the engine's other world; CLOSE PASS has no use for it.

6.3 In-band infrared detection

Telescopes work in NEO Surveyor's NC2 band, 6–10 μm (Mainzer et al. 2023[115] V-TEXT). The in-band share of each body's emission comes from the Widger & Woodall series, which matches astropy to 6×10^{-11}. The 0.5 m LWIR's 1σ noise-equivalent irradiance is 7×10^{-18} W m^{-2}. That lies inside the 0.4–1.1×10^{-17} range derived from NEO Surveyor's S/N-5 sensitivity. A look detects with

```
S/N = I / R² / (NEI × background),     P_d = Φ(S/N − 5)
```

Against the planet's disc, the background raises the NEI ×50, a DESIGN VALUE inside the ×26–92 derived for a background-limited sensor. Just off the disc, stray light raises it ×5, also a design value, out to three times the planet's apparent radius but never more than 20° past its limb. From low orbit the Earth fills almost half the sky, and three times its apparent radius would leave no sky at all; 20° is about the Hubble Space Telescope's bright-Earth avoidance angle. False alarms are Poisson, with a mean of 0.1 per sensor per look (design value), and only lines from two places at once start a track.

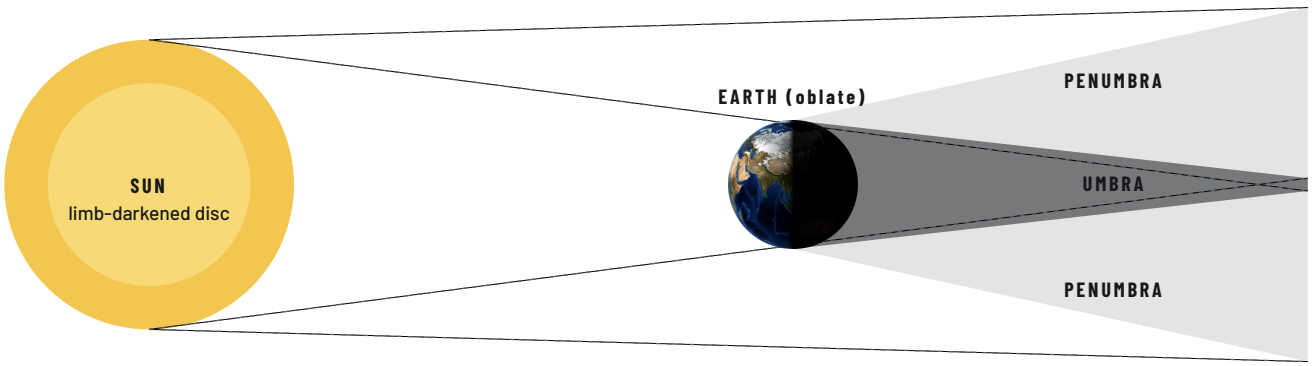
6.4 Shadows and reflected light

The Sun is a limb-darkened disc, $I(\mu) = 1 - u(1 - \mu)$ with $u = 0.6$ (Allen's[106] §14.7), sampled by 397 rays in 12 rings. The sunlit share is the weighted fraction not blocked by the oblate Earth (6,378 × 6,357 km), the Moon, or, far out, a planet. This gives both umbra and penumbra (Montenbruck & Gill §3.4.2), within 0.019 of a dense numerical integration.

Sunlit hulls are also seen in visible light. The Sun's $M_V = 4.81$ (Willmer 2018) is scaled to the irradiance at the craft, and each hull is a Lambert sphere with phase law $\Phi(\alpha) = (\sin\alpha + (\pi - \alpha)\cos\alpha)/\pi$. It returns a share $p\cdot\Phi(\alpha)\cdot r^2/R^2$ of the sunlight at its distance R, with p the geometric albedo and $r^2 = A/4\pi$ for a hull of surface area A (Madhusudhan & Burrows 2012 eq. 3[122]). An earlier build used the cross-section πr^2 in place of r^2, which made every hull π times (1.24 mag) too bright and every visible range $\sqrt{\pi} = 1.77$ times too long. A 1 m

GEODSS-class telescope reaches magnitude 22 (Stokes et al. 1996[119]; the free 1998 Lincoln Laboratory Journal account of the same tests gives magnitude 22 at S/N 4 in under 100 s). The game asks for S/N 5 at magnitude 22, a DESIGN VALUE. Visible telescopes look only where a track already exists, because reaching magnitude 22 takes about 100 s staring at one field.

FIG. 8 **UMBRA AND PENUMBRA**



Schematic, not to scale. 397 rays in 12 rings sample the disc; the share not blocked is the sunlit fraction f.

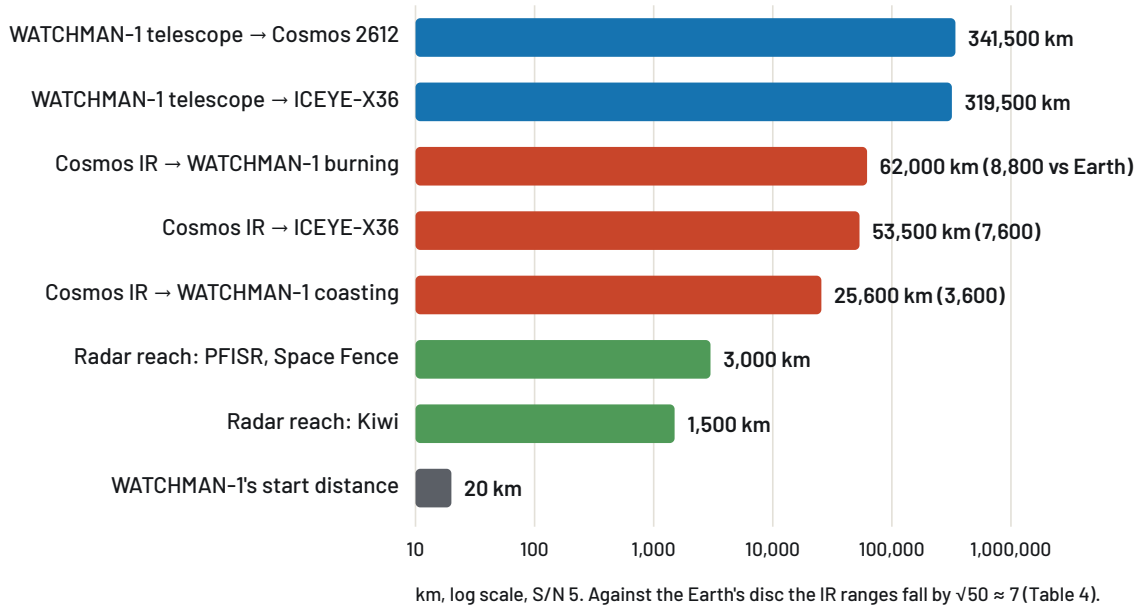
Because the Sun is a disc, the Earth casts a full shadow inside a soft-edged one (§6.4). At 549 km ICEYE-X36 spends up to about 36 minutes of each 95.6-minute orbit in it, depending on the season and its orbit's angle to the Sun.

6.5 What the scenario's sensors see

OBSERVER → TARGET	BAND	AGAINST DEEP SKY	AGAINST THE EARTH
WATCHMAN-1's 0.3 m telescope → Cosmos 2612	Visible, sunlit	341,528	–
WATCHMAN-1's telescope → ICEYE-X36	Visible, sunlit	319,470	–
Cosmos 2612's 0.1 m camera → WATCHMAN-1, coasting	6–10 µm	25,611	3,622
Cosmos 2612's camera → WATCHMAN-1, burning	6–10 µm	61,962	8,763
Cosmos 2612's camera → ICEYE-X36	6–10 µm	53,518	7,569

Table 4. Detection ranges at S/N 5, km, at the start (S = 1,361 W m^{-2}), measured from the engine's own functions. Against the Earth's disc the NEI is ×50, so infrared ranges fall by √50. The telescope looks only where a track already exists (cued), and only at sunlit targets.

FIG. 9 WHO CAN SEE WHOM, AND HOW FAR



From Table 4 and §4.5. Every sensor here outranges the scenario by a wide margin: what limits seeing in CLOSE PASS is geometry (sunlight, the Earth in the way, a radar site's pass), not range.

For the visible ranges the hull is a Lambert sphere (above). With a 1 m telescope the same hulls are seen at 583,270 km (ICEYE-X36), 623,542 km (Cosmos 2612) and 1,150,225 km (WATCHMAN-1), each $\sqrt{(1/0.3)} = 1.83$ times the 0.3 m range, because the limiting flux scales with aperture and flux falls as the square of range. These are long because the Sun at 1 AU is 27 times brighter than at Jupiter.

7 TRACKING

Every contact is a track: an estimate with a covariance, not ground truth. Bearings and ground radar looks (range, azimuth and elevation, §4.5) update it in three dimensions through an unscented Kalman filter (Julier sigma points, $\kappa = 0$, circular mean for angles), which matches filterpy to 3×10^{-12}. Prediction uses central-difference state transition matrices and white-noise acceleration (Bar-Shalom et al. 2001). Two cases needed special handling.

- **Close in.** With WATCHMAN-1 a few kilometres from Cosmos 2612, sigma points can straddle the sensor. Within a tenth of the range, a bearing therefore enters as a pseudo-linear measurement (Lindgren & Gong 1978; Aidala & Nardone 1982). Between craft in nearly the same orbit, range is unobservable from angles alone without a manoeuvre (Woffinden & Geller 2009). So without a recent radar range, the track keeps at least 0.5 × range of 1σ along the line of sight (design value).

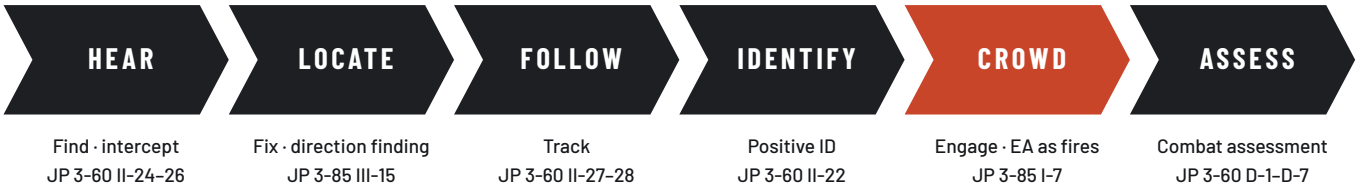
- **Unseen burns.** A bearing whose normalised innovation passes the $\chi^2(1)$ 99.9% point (10.83) is taken as a burn nobody saw, and widens the track (Bar-Shalom ch. 11). The 50 m/s and 10 min used are design values.

CLOSE PASS scores *custody*: Blue's track of Cosmos 2612 within 1 km of the truth for at least 80% of the time (design values). Between radar passes the track coasts on the force model of §3, so custody depends on how well the filter predicts. In the unattended 24-hour run of Fig. 12, with no orders and only the radar sites looking, custody held 94% of the time. Tracks also size the burns they see: a jump in a track's motion is reported as a burn of about so many m/s, give or take its uncertainty.

A track nobody has detected for 24 h, or whose 1σ exceeds 100,000 km, is dropped (after Blackman & Popoli 1999). Both thresholds are design values. Contacts are drawn after MIL-STD-2525D, with a dashed frame for a last known position.

8 DOCTRINE AND THE KILL CHAIN

FIG. 10 THE GAME'S VERBS AS A KILL CHAIN



Each step mapped to its doctrinal term and citation (table below).

The game's verbs follow US joint doctrine, read from the published texts: JP 3-85 *Joint Electromagnetic Spectrum Operations* (2020)[139], JP 3-60 *Joint Targeting* (2018)[141], AFDP 3-60 (2026)[142] and the USSF *Space Warfighting* framework (2025)[143].

GAME STEP	DOCTRINAL TERM	CITATION
Hear	F2T2EA *Find*; electromagnetic support search and intercept	JP 3-60 II-24–26; JP 3-85 I-6
Locate	*Fix*; direction finding, precision geolocation	JP 3-60 II-26–27; JP 3-85 III-15, B-4
Follow	*Track*	JP 3-60 II-27–28
Identify	Positive identification by EW support systems or visual recognition (doctrine acquires it during *Fix*)	JP 3-60 II-22
Crowd	No doctrinal term: a show of presence by an approach that stops short of contact. In the engine's other world this step is *Jam*, doctrine's *Engage* by electromagnetic attack (JP 3-85 I-7, I-13, GL-6, GL-7)	—
Assess	Combat assessment, with confidence graded confirmed, probable or possible	JP 3-60 D-1–D-7

Under JP 3-85, a stealth ship going dark is practising electromagnetic protection: "multispectral low-observability" is one of its listed examples. Doctrine says nothing about TDOA/FDOA, look-through, own-platform jammer isolation, or an escalation ladder. JP 3-85, JP 3-60 and AFDP 3-60 never use the words "spoofing" or "reversible": their terms are intrusion and deception, and temporary or nonlethal effects. (The USSF framework does speak of reversible and nonreversible actions, pp. 5 and 9.) Nor does it treat crowding another craft as an act at all. The tension meter of §5.4 is therefore entirely a design value. Its ordering (reversible and deniable acts cheap, debris-generating acts ruinous) follows doctrine's escalation-of-force guidance qualitatively.

9 THE SCENARIO AND ITS REAL-WORLD BASIS

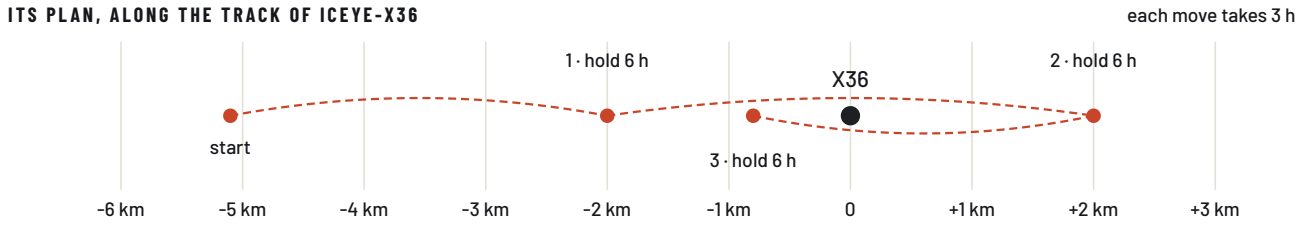
CLOSE PASS is built on a real uncooperative rendezvous and proximity operation. In October 2026 the Russian satellite Cosmos 2612 approached ICEYE-X36, a commercial X-band radar-imaging satellite, and shadowed it at a few kilometres. It was reported from LeoLabs tracking data by Breaking Defense and The War Zone on 19 October 2026[158,159], and reconstructed from public element sets by KeepTrack[168]. As reported, the sequence was: coplanar alignment; closing from long range; station-keeping within 5 km, then 1–2 km; a closest pass reported at 500 m (another report gives 26 m); and moves ahead of and behind the target. The scenario keeps the real craft and their real orbits. WATCHMAN-1, the US inspector the player commands, is notional, and so is everything Cosmos 2612 does after the start.

- **Orbit.** 549 km, a 95.57-minute period, 7.584 km/s (§2.2). Each orbit takes the craft through the Earth's shadow and over different radar sites.
- **Cosmos 2612's plan.** In the order LeoLabs reported the real one: close in from behind to 2 km, reposition 2 km ahead, then loiter 0.8 km behind. Each move takes 3 hours and each slot is held for 6. Distances and

times are DESIGN VALUES.

- **Coming closer.** When no Blue craft is within 50 km of it, it takes its next slot at half the distance, but not under 0.5 km.
- **Giving way.** With a Blue craft within 5 km of it, it gives way to a slot 8 km on the far side of ICEYE-X36. Crowded again after two give-ways (one in the tutorial), it leaves: 4 m/s prograde, and gone once it is beyond 200 km.
- **Its radio.** An S-band (2.25 GHz) BPSK burst at 100 kbaud, 5 W into a 0.3 m dish aimed at its handler near Moscow (the Titov control centre is at Krasnoznamensk), two minutes long, every 3 to 6 hours and after each move. These are design values within ordinary practice.
- **Losing its link.** Cut off from its handler for 3 hours within 200 km of its target, and with a Blue craft within 25 km of it, it leaves. Cut off but alone, it holds its slot and waits. This is grounded in practice, not in a published rule: a Progress approach to the ISS was aborted on loss of its telemetry link in 2010[162], and ESA's ATV carried RETREAT and ESCAPE modes for the same reason. The threshold and the burn are DESIGN VALUES.
- **Score.** Making it break off counts 40; keeping it outside 1 km of ICEYE-X36, 20; custody, 20; using no more than half of WATCHMAN-1's fuel, 10; staying below open conflict, 10. Design values.
- **Timescale.** The real event took weeks. The scenario runs two days from 21:00 UTC on 26 October 2026 DESIGN VALUE.

FIG. 11 HOW COSMOS 2612 BEHAVES



WHAT CHANGES ITS PLAN

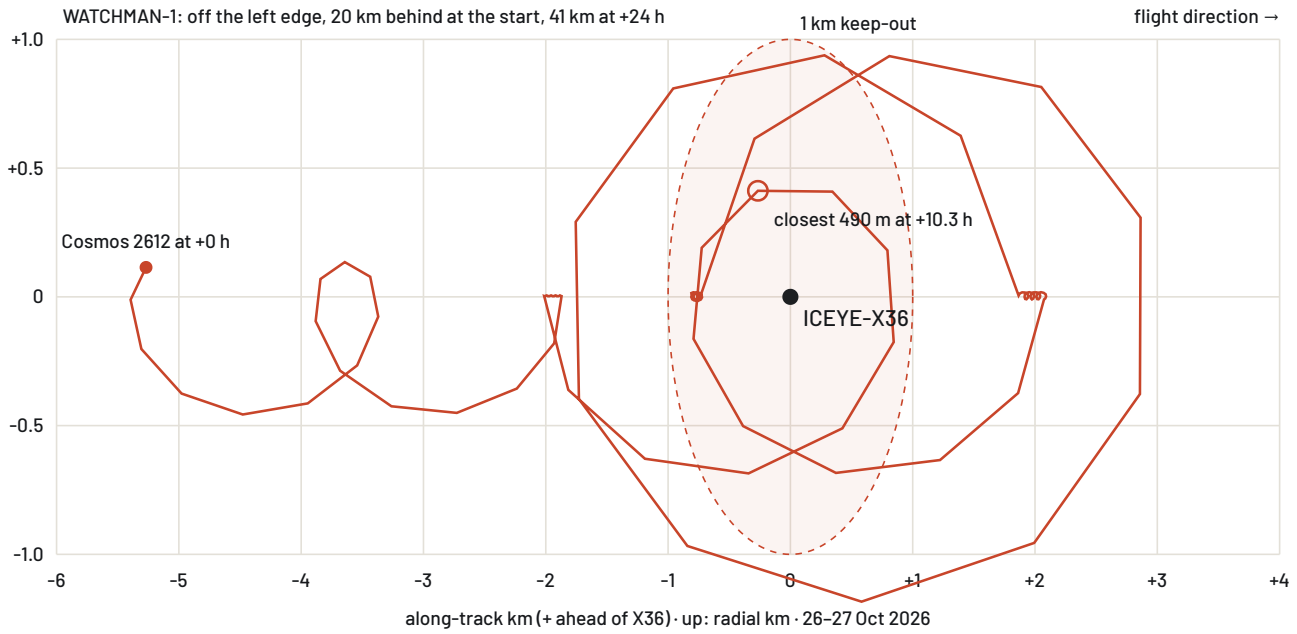
No Blue craft within 50 km	takes its next slot at half the distance (not under 0.5 km)
Blue within 5 km of it	gives way to a slot 8 km on the far side of X36
Crowded again after 2 give-ways	leaves: +4 m/s prograde, gone beyond 200 km
Cut off from its handler 3 h, Blue within 25 km	leaves; cut off but alone, it waits

Top: its plan along ICEYE-X36's track (§9). Bottom: what makes it come closer, give way or leave. Every threshold is a DESIGN VALUE.

Left alone, the plan runs to completion. Fig. 12 is a real 24-hour run of the engine with no orders given: Cosmos 2612 parks 2 km behind ICEYE-X36 at +3 h, passes within 490 m of it at +10.3 h on its way to its slot 2

km ahead (+11.5 h), and at +19.8 h parks 0.8 km behind, inside the keep-out. The keep-out objective fails, while WATCHMAN-1, given no orders, drifts from 20 km to 41 km behind.

FIG. 12 CLOSE PASS LEFT ALONE FOR 24 HOURS



A real Core run (`cli/run.gd --hours=24 --step=600`, seed 4417, no orders), plotted from its debrief: Cosmos 2612's position relative to ICEYE-X36 every 10 minutes. It works through its plan and comes within 490 m at +10.3 h, inside the 1 km keep-out. Blue's track held within 1 km 94% of the time.

10 VERIFICATION

A Godot script runs every test case through the engine's own functions and writes the results out. A Python suite (pytest) then compares them with independent references, each comparison carrying its own tolerance. JPL data is cached, so the suite runs offline. The suite exercises the engine on its own world, at Jupiter, where JPL Horizons gives an exact reference for every body; the models are the same ones CLOSE PASS runs at the Earth. On 1 November 2026 it made 681 comparisons across 64 tests; all 681 fall within tolerance, and 4 further rows report known simplifications.

MODEL	REFERENCE	TOLERANCE	WORST RESULT
Kepler propagation (94 cases, e to 0.999 and hyperbolic)	hapsira farnocchia; scipy DOP853	1e-8	7.1e-10
Lambert (111 transfers)	hapsira izzo	1e-6	7.3e-15
Worked examples	Curtis Ex. 3.7, 5.2; Vallado Ex. 2-4	½ last digit	pass
Force model (J2, third bodies)	hapsira perturbations; gradient of the J2 potential	1e-9	8.5e-11
DOP853 integration, 1 day	scipy DOP853, rtol 1e-13	1 cm	2.8 mm
J2 secular rates	Vallado eqs. 9-41/42	1%	0.40%
Galilean moons, Sun and planets	JPL Horizons	per body	pass
Antenna patterns (468 cases)	ITU-R SA.509-3, S.465-5, coded from the text	1e-9 dB	1.4e-14
Free-space loss	ITU-R P.525-4 eq. (4), 32.4 dB constant	0.05 dB	0.048 dB
Radiometer gain $\sqrt{(B\tau)}$	Monte Carlo energy detector	6%	1.5%
Interferometer DF σ	Monte Carlo two-element correlator	8%	3%
Radar SNR and monopulse angle	Skolnik; Barton	1e-9; 0.2%	5.6e-15; 0.14%
Jammer J/S and reach	Adamy, independent dB form; brentq	1e-9 dB	5.7e-14
Radiators against JIMO	Siamidis 2005 design point	2%	1.1%
Shadow fraction	Dense numpy disc integration	0.02	0.019
Skin heat capacity	scipy solve_ivp	0.05 K	0.0001 K
Unscented update	filterpy UKF	1e-6	3.3e-12
Rocket equation	Tsiolkovsky, every ship	0.006 km/s	0.0032 km/s

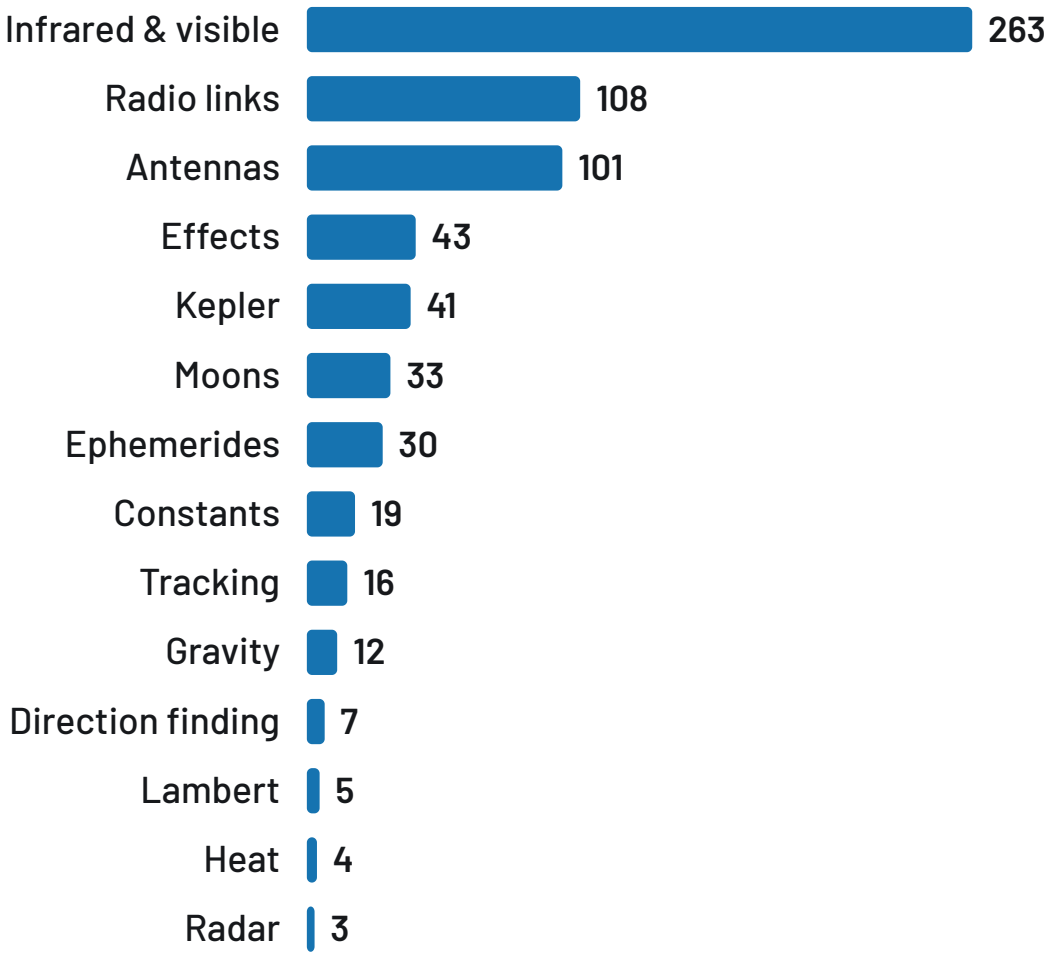
Table 5. Selected comparisons. The full table has one row per comparison.

The Earth's own numbers are checked by two Godot tests, `earth_test` and `close_pass_earth_test`, against textbook values. Both pass:

CHECK	ENGINE	REFERENCE
ICEYE-X36's node turns per day	1.0395°	1.0400°, J2's first-order secular rate (Vallado eqs. 9-41/42)
A craft on the no-drift path beside it, over one orbit	within 779 m	under 800 m: starting states and forces agree
The Sun's distance at the start	0.9938 AU	0.98–1.00 AU in late October
PFISR's speed on the turning Earth	0.1962 km/s	0.1961 km/s: ω × distance from the axis at 65.1° N on WGS 84
A station 1 km out of ICEYE-X36's plane	held at 1.00 km	1 km
A 3 h move from 20 km to ICEYE-X36	0.75 m/s flown	0.74 m/s planned
WATCHMAN-1's Δv	259 m/s	Tsiolkovsky: 2.2 km/s × ln(675/600)

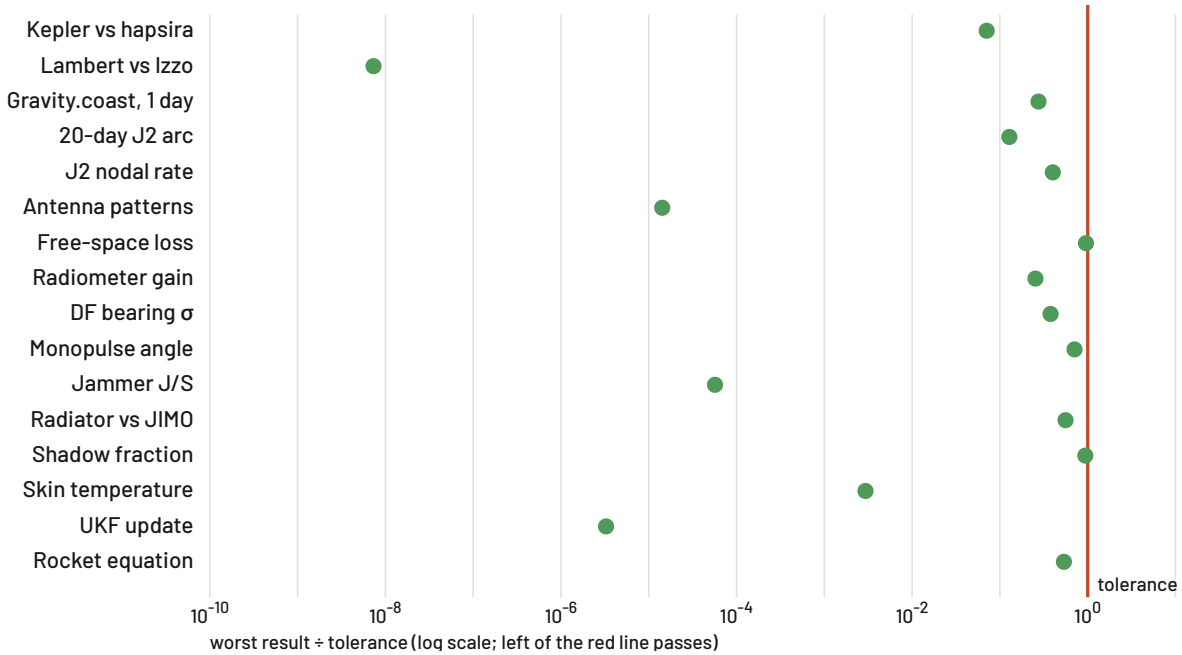
Table 5b. Checks of CLOSE PASS at the Earth.

FIG. 13 **WHERE THE 685 ROWS GO**



Rows per domain on 1 November 2026: 681 within tolerance, and 4 that report known simplifications.

FIG. 14 **HOW MUCH MARGIN EACH CHECK HAS**



Worst result divided by its tolerance, for the numeric rows of Table 5. Every dot sits left of the red line; most sit orders of magnitude inside it.

The suite has also found and fixed real errors. Moon longitudes were up to 114° off. DF σ was three times too large, because it was fed the integrated SNR. The barrage band was twice as wide as the real allocation. Long-way Lambert transfers failed. Two hulls were π times too bright in visible light. And the check of who sees whom had to learn the 20° cap on glare that the Earth brought in (§6.3). Kepler's equation lost accuracy near e = 1. Each fix and its effect on play is recorded in the project's verification log.

11 LIMITS, SIMPLIFICATIONS AND OPEN QUESTIONS

Not public, so notional

- Cosmos 2612's mass, engine, propellant, camera and radio. Only its orbit and its observed moves are public.
- WATCHMAN-1 as a whole. GSSAP's mass is reported; its sizes, thrusters and sensors were never published.
- Angle noise and elevation masks of the radar sites, and all of Space Fence's figures.
- The site and mask of Cosmos 2612's handler.

Not verified

- The closest approach of the real event: one report gives 500 m, another 26 m.
- HawkEye 360 geolocation accuracy; the Albersheim validity limits; specific-emitter identification accuracy; look-through duty cycles.
- The 2024 edition of JP 3-60 (the 2018 edition was read), and JP 5-0's definitions of MOE and MOP.
- MIL-STD-2525D was read through a reproduction of its tables, not the original PDF.

Simplifications

- No atmospheric drag. At 549 km it slows a small satellite by metres per second per year, depending on the Sun's activity; over two days it moves the three craft relative to each other by an amount that depends on their area-to-mass ratios, which are not public.
- No reflected sunlight or infrared from the Earth in the heat balance, though the Earth's disc does raise the infrared background (§6.3).
- A low-precision Moon (a few arcminutes) and an approximate Sun; no Earth gravity terms beyond J2.
- No nutation, polar motion or UT1 − UTC: ground sites sit within about 1 km of their true places.
- SGP4 is used only for the starting state; nothing is fitted back to element sets during play.
- The umpire's view: some kill-chain indicators still read ground truth rather than Blue's assessed belief.

---

12 xGEO CORE AS AN OPEN-SOURCE TOOL

The models in this edition make up **xGEO Core**, the engine under the game. **xGEO Live**, the game, draws what Core computes and sends orders into it, and nothing more. Core runs with no window, and it is being prepared for release as an open-source simulation tool for teaching, concept studies and research. It is not a validated operational tool.

12.1 What is Core and what is Live

PART	WHAT IT HOLDS	WHERE
Core: physical models	Two-body motion, Lambert, gravity with J2 and third bodies, ephemerides, SGP4 starting states, the turning Earth and ground sites, link budgets, antenna patterns, radar, heat and infrared, the heat forecast, sensing, the tracking filter, breakup and debris, civil traffic, and the world that ties them together	`godot/core/`
Core: scenario rules	Blue's effects and their costs, Red's behaviour, objectives and the debrief, the log's wording, save and continue. They run headless, but they are rules of play, and most of their values are Notional	`godot/core/`
Scenarios	Classes, equipment and constants; CLOSE PASS's craft, radar sites, Red's plan and objectives	`godot/data/*.json`
Live	The console, the map, the windows, art, sound, the tutorial	`godot/ui/`, `godot/scenes/`, `godot/assets/`

Table 6. The split. A check in the test suite fails if anything in Core names one of Live's classes.

12.2 Running Core without the game

A command-line runner loads a scenario, steps time and writes what happens as JSON lines, one object per line:

```
godot --headless --path godot --script res://cli/run.gd -- \
      --hours=24 --step=600 --seed=4417 --out=run.jsonl
```

The first line describes the run (scenario, seed, start time, units). Each step line carries the time, escalation, Blue's ships (position, velocity and Δv left), Blue's tracks with their 1σ ellipses, and every log entry since the last step. The last line is the debrief. Tracks report Blue's belief, never the truth; `--truth=true` adds the true states for analysis. Units are kilometres, km/s and seconds, centred on the scenario's central body: the Earth in CLOSE PASS. Run with no scenario, Core loads its own sample world at Jupiter. The test suite runs it on every change.

12.3 Real, Projected and Notional

Every model and value carries one of three labels, which extend the source labels of §1:

- **Real:** sourced and checked against an independent reference (§10). The orbits, gravity, the radio and radar equations, Planck's law, the filter.

- **Projected:** near-future and grounded in programmes that exist today, such as nuclear-thermal drives at NASA's tested 900 s specific impulse.
- **Notional:** invented for a scenario, the way defence and industry studies fly notional systems: Red's classes and behaviour, equipment sizes, escalation scores, the compressed timescale.

A Real model fed Notional inputs gives a Notional answer: the jamming equation is exact, but a Red jammer's power is a design value, and so is the range it yields. The project's fidelity table (`docs/FIDELITY.md`) gives each model's label, what it was checked against and what it leaves out.

12.4 Status of the release

Licence (26 October 2026): xGEO Core, the code of the models, the runner, the tests and the verification, is released under the Apache License 2.0. Anyone may use it and change their own copy for any purpose, keeping the notices and not calling their version xGEO. The game, its art and story, and this document stay all rights reserved. Core is open source but not open to contributions: bug reports, physics corrections and feature requests are welcome as issues; pull requests are not accepted. Done: the asset licence audit, the Core and Live split with its check, the command-line runner, the fidelity table, and contribution, conduct and security guides. The jamming and counterspace models are built only from open, published sources, every one cited in this edition, and the owner has cleared them and the name for release. CLOSE PASS names real satellites, operators and radar sites from public records; WATCHMAN-1 and everything the scenario has them do after its start are notional. Still to do before release: a review of the repository's history, then making it public. Issues must cite public sources only.

REFERENCES

Every source the game cites, in its code, data and tests, grouped by the model that uses it. A link opens the document itself, or a free copy where the publisher's is behind a paywall. Works with no readable copy online are listed without one.

EPHEMERIDES AND REFERENCE FRAMES §2

1. JPL Solar System Dynamics Group. Horizons On-Line Ephemeris System. Jet Propulsion Laboratory, California Institute of Technology. JPL SSD ↗
2. Standish, E. M. & Williams, J. G. (1992). Keplerian Elements for Approximate Positions of the Major Planets. JPL Solar System Dynamics (web edition). JPL SSD ↗
3. Park, R. S., Folkner, W. M., Williams, J. G. & Boggs, D. H. (2021). The JPL Planetary and Lunar Ephemerides DE440 and DE441. Astronomical Journal 161(3):105. doi:10.3847/1538-3881/abd414 JPL SSD PDF ↗

4. JPL Solar System Dynamics. Planetary Satellite Mean Elements (Jupiter: JUP365). JPL SSD ↗

5. JPL Solar System Dynamics. Planetary Satellite Physical Parameters. JPL SSD ↗

6. Jacobson, R. A. (2021). The Orbits of the Regular Jovian Satellites and the Orientation of the Pole of Jupiter (JUP365). Personal communication to Horizons/NAIF. Corroborated by: JPL Solar System Dynamics, Planetary Satellite Mean Elements (JUP365), which gives this reference JPL SSD ↗ .

7. Archinal, B. A., Acton, C. H., A'Hearn, M. F. et al. (2018). Report of the IAU Working Group on Cartographic Coordinates and Rotational Elements: 2015. Celestial Mechanics and Dynamical Astronomy 130(3):22. doi:10.1007/s10569-017-9805-5 Corroborated by: NAIF/JPL (2022). Generic PCK kernel pck00011.tpc (IAU WGCCRE 2015 constants, citing Archinal et al. 2018) NAIF ↗ ; Archinal, B. A. et al. (2019). Correction to: Report of the IAU WGCCRE: 2015. CMDA 131:61 (DLR repository copy) ELIB.DLR.DE PDF ↗ .

8. IAU (2015). Resolution B3 on recommended nominal conversion constants for selected solar and planetary properties. XXIXth IAU General Assembly, Honolulu. See also Prša, A. et al. (2016). Nominal values for selected solar and planetary quantities: IAU 2015 Resolution B3. Astronomical Journal 152(2):41. IAU.ORG PDF ↗

9. Williams, D. R. Jupiter Fact Sheet. NASA Space Science Data Coordinated Archive (NSSDCA), Goddard Space Flight Center. NSSDC.GSFC.NASA.GOV ↗

10. Williams, D. R. Jovian Satellite Fact Sheet. NASA Space Science Data Coordinated Archive (NSSDCA), Goddard Space Flight Center. NSSDC.GSFC.NASA.GOV ↗

11. Peale, S. J. (1976). Orbital resonances in the solar system. Annual Review of Astronomy and Astrophysics 14:215–246. ADS SCAN PDF ↗ Corroborated by: Peale, S. J. & Lee, M. H. (2002). A primordial origin of the Laplace relation among the Galilean satellites. Science 298:593 (arXiv:astro-ph/0210589) ARXIV ↗ .

12. Peale, S. J., Cassen, P. & Reynolds, R. T. (1979). Melting of Io by tidal dissipation. Science 203(4383):892–894. Corroborated by: Morabito, L. A. (2012). Discovery of volcanic activity on Io: a historical review. arXiv:1211.2554 ARXIV ↗ .

GRAVITY AND TRAJECTORIES

§3

13. Folkner, W. M., Iess, L., Anderson, J. D. et al. (2017). Jupiter gravity field estimated from the first two Juno orbits. Geophysical Research Letters 44(10):4694–4700. doi:10.1002/2017GL073140 IRIS.UNIROMA1.IT PDF ↗

14. Iess, L., Folkner, W. M., Durante, D. et al. (2018). Measurement of Jupiter's asymmetric gravity field. Nature 555:220–222. doi:10.1038/nature25776 WEIZMANN.AC.IL PDF ↗

15. Durante, D., Parisi, M., Serra, D. et al. (2020). Jupiter's gravity field halfway through the Juno mission. Geophysical Research Letters 47(4):e2019GL086572. doi:10.1029/2019GL086572 CRIS.UNIBO.IT PDF ↗

16. Sicardy, B. (2010). Stability of the triangular Lagrange points beyond Gascheau's value. Celestial Mechanics and Dynamical Astronomy 107(1–2):145–155. doi:10.1007/s10569-010-9259-5 HAL ↗

17. Curtis, H. D. (2020). Orbital Mechanics for Engineering Students, 4th ed. Butterworth-Heinemann (Elsevier). Corroborated by: Weber, B. Orbital Mechanics & Astrodynamics (open textbook, CC BY-SA 4.0) OPEN TEXTBOOK ↗ ; Izzo, D. (2015). Revisiting Lambert's problem. CMDA 121:1-15 (arXiv:1403.2705) ARXIV ↗ ; NASA/TP-20220014814 (2022). Astrodynamics Convention and Modeling Reference for Lunar, Cislunar, and Libration Point Orbits. NASA NASA NTRS ↗ ; JPL SSD, Approximate Positions of the Planets (Standish & Williams 1992 web edition) JPL SSD ↗ .

18. Vallado, D. A. (2013). Fundamentals of Astrodynamics and Applications, 4th ed. Microcosm Press. Corroborated by: hapsira (open-source poliastro fork), core/propagation/vallado.py, documented as Vallado's KEPLER algorithm GITHUB ↗ ; NASA/TP-20220014814 (2022). Astrodynamics Convention and Modeling Reference for Lunar, Cislunar, and Libration Point Orbits. NASA NASA NTRS ↗ .

19. Bate, R. R., Mueller, D. D. & White, J. E. (1971). Fundamentals of Astrodynamics. Dover Publications. Corroborated by: Weber, B. Orbital Mechanics & Astrodynamics (open textbook, CC BY-SA 4.0) OPEN TEXTBOOK ↗ .

20. Montenbruck, O. & Gill, E. (2000). Satellite Orbits: Models, Methods and Applications. Springer. Corroborated by: NASA/TP-20220014814 (2022). Astrodynamics Convention and Modeling Reference for Lunar, Cislunar, and Libration Point Orbits. NASA NASA NTRS ↗ .

21. Aarseth, S. J. (2003). Gravitational N-Body Simulations: Tools and Algorithms. Cambridge University Press. Corroborated by: Pelupessy, F. I., Jaenes, J. & Portegies Zwart, S. (2012). N-body integrators with individual time steps from hierarchical splitting. New Astronomy 17:711 (arXiv:1205.5668) ARXIV ↗ .

22. Danby, J. M. A. (1987). The solution of Kepler's equation. III. Celestial Mechanics 40:303–312. ADS SCAN PDF ↗ Corroborated by: Zechmeister, M. (2018). CORDIC-like method for solving Kepler's equation. A&A 619:A128 (arXiv:1808.07062) ARXIV ↗ .

23. Izzo, D. (2015). Revisiting Lambert's problem. Celestial Mechanics and Dynamical Astronomy 121(1):1–15. doi:10.1007/s10569-014-9587-y ARXIV ↗

24. Broyden, C. G. (1965). A class of methods for solving nonlinear simultaneous equations. Mathematics of Computation 19(92):577–593. AMS.ORG PDF ↗ Corroborated by: Bindel, D. (2023). CS 4220 Numerical Analysis, lecture notes 2023-04-14 'Broyden'. Cornell University CS.CORNELL.EDU PDF ↗ .

25. Press, W. H., Teukolsky, S. A., Vetterling, W. T. & Flannery, B. P. (1992). Numerical Recipes in C: The Art of Scientific Computing, 2nd ed. Cambridge University Press. NR.COM READER ↗

26. Press, W. H., Teukolsky, S. A., Vetterling, W. T. & Flannery, B. P. (2007). Numerical Recipes: The Art of Scientific Computing, 3rd ed. Cambridge University Press. NUMERICAL.RECIPES ↗ Corroborated by: Bindel, D. (2023). CS 4220 lecture notes 'Broyden'. Cornell University CS.CORNELL.EDU PDF ↗ .

PROPULSION

§3

27. NASA Glenn Research Center. Ideal Rocket Equation. Beginner's Guide to Aeronautics (formerly Beginner's Guide to Rockets). GRC.NASA.GOV ↗

28. Tsiolkovsky, K. E. (1903). Exploration of Outer Space by Means of Reaction Devices [Issledovanie mirovykh prostranstv reaktivnymi priborami]. Nauchnoe Obozrenie, no. 5. English translation as 'A Rocket into Cosmic Space (1903)' in Works on Rocket Technology, NASA TT F-243 (1965). TSIOLKOVSKY.ORG PDF ↗

29. Sutton, G. P. & Biblarz, O. (2016). Rocket Propulsion Elements, 9th ed. Wiley. Corroborated by: Reed, B. D. (2004). On-board chemical propulsion technology. NASA/TM-2004-212698, NASA Glenn NASA NTRS ↗ .

30. Borowski, S. K., McCurdy, D. R. & Packard, T. W. (2009). Nuclear Thermal Rocket/Vehicle Characteristics and Sensitivity Trades for NASA's Mars Design Reference Architecture (DRA) 5.0 Study. Nuclear and Emerging Technologies for Space (NETS) 2009, Atlanta. NTRS 20120012928. NASA NTRS ↗

31. Borowski, S. K., McCurdy, D. R. & Packard, T. W. (2012). Nuclear Thermal Propulsion (NTP): A Proven Growth Technology for Human NEO/Mars Exploration Missions. IEEE Aerospace Conference, Big Sky, MT; NASA report E-18081, NTRS 20120003776. NASA NTRS ↗

32. NASA (2023, January 24). NASA, DARPA Will Test Nuclear Engine for Future Mars Missions [news release]. Demonstration Rocket for Agile Cislunar Operations (DRACO), a DARPA/NASA program. NASA.GOV ↗

RADIO: ANTENNAS, LINKS AND DETECTION

§4

33. ITU-R Recommendation SA.509-3 (12/2013). Space research earth station and radio astronomy reference antenna radiation pattern for use in interference calculations, including coordination procedures, for frequencies less than 30 GHz. ITU, Geneva. ITU PDF ↗

34. ITU-R Recommendation S.465-5 (1993). Reference earth-station radiation pattern for use in coordination and interference assessment in the frequency range from 2 to about 30 GHz. ITU,

Geneva. (Superseded by S.465-6, 01/2010.) ITU PDF ↗

35. ITU-R Recommendation S.1428-1 (02/2001). Reference FSS earth-station radiation patterns for use in interference assessment involving non-GSO satellites in frequency bands between 10.7 GHz and 30 GHz. ITU, Geneva. ITU PDF ↗

36. ITU-R Recommendation S.672-4 (09/1997). Satellite antenna radiation pattern for use as a design objective in the fixed-satellite service employing geostationary satellites. ITU, Geneva. ITU PDF ↗

37. ITU-R Recommendation P.525-4 (08/2019). Calculation of free-space attenuation. ITU, Geneva. (Superseded by P.525-5, 11/2024.) ITU PDF ↗

38. ITU-R Recommendation SM.1055-0 (07/1994). The use of spread spectrum techniques. ITU, Geneva. ITU PDF ↗

39. JPL. DSN Telecommunications Link Design Handbook, 810-005: Module 201, Frequency and Channel Assignments, Rev. F (May 2022); Module 202, Doppler Tracking, Rev. D (Sept. 2021); Module 104, 34-m BWG Stations Telecommunications Interfaces, Rev. O (34 m X-band gain, Table 8; system temperatures, Table 11). Jet Propulsion Laboratory, Pasadena. JPL PDF ↗

40. CCSDS 401.0-B-32 (October 2021). Radio Frequency and Modulation Systems, Part 1: Earth Stations and Spacecraft. Recommended Standard (Blue Book), Issue 32. CCSDS, Washington, DC. CCSDS PDF ↗

41. IEEE Std 211-2018. IEEE Standard Definitions of Terms for Radio Wave Propagation. IEEE, New York (revision of IEEE Std 211-1997). Corroborated by: ITU-R P.372-17 (08/2024). Radio noise ITU PDF ↗.

42. Friis, H. T. (1946). A note on a simple transmission formula. Proceedings of the IRE 34(5):254-256. doi:10.1109/JRPROC.1946.234568 Corroborated by: Naval Air Warfare Center Weapons Division (2013). Electronic Warfare and Radar Systems Engineering Handbook, 4th ed., NAWCWD TP 8347 (DTIC ADA617071) EVERYSPEC.COM ↗.

43. Shannon, C. E. (1949). Communication in the presence of noise. Proceedings of the IRE 37(1):10-21. doi:10.1109/JRPROC.1949.232969 Corroborated by: Modiano, E. MIT OCW 16.36 Communication Systems Engineering (Spring 2009), Lecture 2 MIT OCW ↗.

44. Balanis, C. A. (2016). Antenna Theory: Analysis and Design, 4th ed. Wiley, Hoboken, NJ. Corroborated by: ITU-R P.525-4 (08/2019). Calculation of free-space attenuation ITU PDF ↗; Naval Air Warfare Center Weapons Division (2013). Electronic Warfare and Radar Systems Engineering Handbook, 4th ed., NAWCWD TP 8347 (DTIC ADA617071) EVERYSPEC.COM ↗.

45. Skolnik, M. I. (2001). Introduction to Radar Systems, 3rd ed. McGraw-Hill, New York.

46. Skolnik, M. I. (ed.) (2008). Radar Handbook, 3rd ed. McGraw-Hill, New York. Corroborated by: Naval Air Warfare Center Weapons Division (2013). Electronic Warfare and Radar Systems Engineering

Handbook, 4th ed., NAWCWD TP 8347 (DTIC ADA617071) EVERYSPEC.COM ↗ ; ITU-R SA.509-3 (12/2013) ITU PDF ↗ .

47. Barton, D. K. (2005). Radar System Analysis and Modeling. Artech House, Norwood, MA. Corroborated by: MIT Lincoln Laboratory, Introduction to Radar Systems lecture series: Tracking and Parameter Estimation (2008) MIT LL ↗ .

48. Richards, M. A. (2005). Fundamentals of Radar Signal Processing. McGraw-Hill, New York.

49. Albersheim, W. J. (1981). A closed-form approximation to Robertson's detection characteristics. Proceedings of the IEEE 69(7):839. doi:10.1109/PROC.1981.12082 Corroborated by: Naval Air Warfare Center Weapons Division (2013). Electronic Warfare and Radar Systems Engineering Handbook, 4th ed., NAWCWD TP 8347 (DTIC ADA617071) EVERYSPEC.COM ↗ .

50. North, D. O. (1963). An analysis of the factors which determine signal/noise discrimination in pulsed-carrier systems. Proceedings of the IEEE 51(7):1016-1027 (reprint of RCA Laboratories Report PTR-6C, June 1943). doi:10.1109/PROC.1963.2383

51. Urkowitz, H. (1967). Energy detection of unknown deterministic signals. Proceedings of the IEEE 55(4):523-531. doi:10.1109/PROC.1967.5573 Corroborated by: Rashid, M. & Nanzer, J. A. (2024). Expectation Maximization Aided Modified Weighted Sequential Energy Detector for Distributed Cooperative Spectrum Sensing. arXiv:2403.19556 ARXIV PDF ↗ ; Condon, J. J. & Ransom, S. M. Essential Radio Astronomy, ch. 3 (NRAO / Princeton Univ. Press 2016, online edition) NRAO ↗ .

52. Dicke, R. H. (1946). The measurement of thermal radiation at microwave frequencies. Review of Scientific Instruments 17(7):268-275. doi:10.1063/1.1770483 Corroborated by: Condon, J. J. & Ransom, S. M. Essential Radio Astronomy, ch. 3 (NRAO / Princeton Univ. Press 2016, online edition) NRAO ↗ .

53. Wilson, T. L., Rohlfs, K. & Hüttemeister, S. (2013). Tools of Radio Astronomy, 6th ed. Springer, Berlin. Corroborated by: Condon, J. J. & Ransom, S. M. Essential Radio Astronomy, ch. 3 (NRAO / Princeton Univ. Press 2016, online edition) NRAO ↗ .

54. Naval Air Warfare Center Weapons Division (2013). Electronic Warfare and Radar Systems Engineering Handbook, 4th ed., NAWCWD TP 8347. Point Mugu, CA. (DTIC ADA617071, approved for public release.) DTIC PDF ↗

55. Kerczewski, R. J., Yu, J., Walton, J. C., Perl, T. D., Andro, M. & Alexovich, R. E. (1992). Multiple-access phased array antenna simulator for a digital beam forming system investigation. NASA TM-105422 (Ninth International Conference on Digital Satellite Communications, Copenhagen, May 1992). NASA NTRS PDF ↗

56. Gardner, W. A. (1991). Exploitation of spectral redundancy in cyclostationary signals. IEEE Signal Processing Magazine 8(2):14-36. doi:10.1109/79.81007 CYCLOSTATIONARITY.COM PDF ↗

57. Self, A. G. & Smith, B. G. (1985). Intercept time and its prediction. IEE Proceedings F (Communications, Radar and Signal Processing) 132(4):215. doi:10.1049/ip-f-1.1985.0052

58. Clarkson, I. V. L., Perkins, J. E. & Mareels, I. M. Y. (1996). Number/theoretic solutions to intercept time problems. IEEE Transactions on Information Theory 42(3):959-971. doi:10.1109/18.490557

59. Wiley, R. G. (2006). ELINT: The Interception and Analysis of Radar Signals. Artech House, Norwood, MA.

60. Pace, P. E. (2009). Detecting and Classifying Low Probability of Intercept Radar, 2nd ed. Artech House, Norwood, MA.

61. Torrieri, D. (2022). Principles of Spread-Spectrum Communication Systems, 5th ed. Springer, Cham.

62. Donkersley, J. (with Rouma, A.) (2022). SDR++ User Guide, for SDR++ up to version 1.1. SDR++ software by Alexandre Rouma. SDRPP.ORG PDF ↗

63. GNU Radio Foundation / SigMF project. Signal Metadata Format (SigMF) Specification, version 1.2.x (v1.2.6 current). SIGMF.GITHUB.IO ↗

64. AMD (2023). Zynq UltraScale+ RFSoC Data Sheet: Overview, DS889 (v1.14), 27 June 2023. DOCS.AMD.COM ↗

DIRECTION FINDING AND GEOLOCATION §4

65. Knapp, C. H. & Carter, G. C. (1976). The generalized correlation method for estimation of time delay. IEEE Transactions on Acoustics, Speech, and Signal Processing 24(4):320-327. doi:10.1109/TASSP.1976.1162830 Corroborated by: Obo, H. et al. (2025). Noise Suppression for Time Difference of Arrival: Performance Evaluation of a Generalized Cross-Correlation Method Using Mean Signal and Inverse Filter. arXiv:2512.05355 ARXIV PDF ↗ .

66. Thompson, A. R., Moran, J. M. & Swenson, G. W., Jr. (2017). Interferometry and Synthesis in Radio Astronomy, 3rd ed. Astronomy and Astrophysics Library, Springer, Cham. doi:10.1007/978-3-319-44431-4 SPRINGER (OPEN) ↗

67. Poisel, R. A. (2012). Electronic Warfare Target Location Methods, 2nd ed. Artech House, Norwood, MA. Corroborated by: Thompson, A. R., Moran, J. M. & Swenson, G. W. (2017). Interferometry and Synthesis in Radio Astronomy, 3rd ed., Springer (open access) SPRINGER (OPEN) PDF ↗ ; Herath, S. C. & Pathirana, P. N. (2013). Optimal sensor arrangements in Angle of Arrival (AoA) and range based localization with linear sensor arrays. Sensors 13(9):12277-12294. doi:10.3390/s130912277 (open access, PMC3821368) PMC (OPEN) ↗ .

68. Stein, S. (1981). Algorithms for ambiguity function processing. IEEE Transactions on Acoustics, Speech, and Signal Processing 29(3):588-599. doi:10.1109/TASSP.1981.1163621 Corroborated by: Fowler, M. L. EECE 522 Notes 15: ML for TDOA/FDOA (revised). Binghamton University course notes

WS2.BINGHAMTON.EDU PDF ↗ ; Obo, H. et al. (2025), arXiv:2512.05355 (Knapp & Carter coherence CRLB) ARXIV PDF ↗ .

69. Ho, K. C. & Chan, Y. T. (1997). Geolocation of a known altitude object from TDOA and FDOA measurements. IEEE Transactions on Aerospace and Electronic Systems 33(3):770-783. doi:10.1109/7.599239

70. Ho, K. C. & Xu, W. (2004). An accurate algebraic solution for moving source location using TDOA and FDOA measurements. IEEE Transactions on Signal Processing 52(9):2453-2463. doi:10.1109/TSP.2004.831921

71. Ho, K. C., Lu, X. & Kovavisaruch, L. (2007). Source localization using TDOA and FDOA measurements in the presence of receiver location errors: analysis and solution. IEEE Transactions on Signal Processing 55(2):684-696. doi:10.1109/TSP.2006.885744

72. Sarda, K., Roth, N., Zee, R. E., CaJacob, D. & Orr, N. G. (2018). Making the invisible visible: precision RF-emitter geolocation from space by the HawkEye 360 Pathfinder mission. 32nd Annual AIAA/USU Conference on Small Satellites, Logan, UT, paper SSC18-II-06. (Also presented at IAC 2018 as IAC-18-B4.4.1.) SMALLSAT 2018 PDF ↗

73. ESA eoPortal. HawkEye 360 (satellite mission page). EOPORTAL.ORG ↗

74. Burt, E. A., Prestage, J. D., Tjoelker, R. L. et al. (2021). Demonstration of a trapped-ion atomic clock in space. Nature 595:43-47. doi:10.1038/s41586-021-03571-7

ELECTROMAGNETIC ATTACK AND DIRECTED ENERGY §5

75. Adamy, D. L. (2001). EW 101: A First Course in Electronic Warfare; (2004) EW 102: A Second Course in Electronic Warfare; (2009) EW 103: Tactical Battlefield Communications Electronic Warfare. Norwood, MA: Artech House. Corroborated by: Naval Air Warfare Center Weapons Division (2013). Electronic Warfare and Radar Systems Engineering Handbook, NAWCWD TP 8347, 'Support Jamming' section (public domain; RF Cafe reproduction) RFCAFE.COM ↗ .

76. Cummings, W. C. (1992). An adaptive nulling antenna for military satellite communications. The Lincoln Laboratory Journal 5(2):173–194. MIT LL PDF ↗

77. Sabharwal, A., Schniter, P., Guo, D., Bliss, D. W., Rangarajan, S. & Wichman, R. (2014). In-band full-duplex wireless: challenges and opportunities. IEEE Journal on Selected Areas in Communications 32(9):1637–1652. doi:10.1109/JSAC.2014.2330193 ARXIV ↗

78. Danev, B., Zanetti, D. & Čapkun, S. (2012). On physical-layer identification of wireless devices. ACM Computing Surveys 45(1), article 6:1–29. doi:10.1145/2379776.2379782

79. Riyaz, S., Sankhe, K., Ioannidis, S. & Chowdhury, K. (2018). Deep learning convolutional neural networks for radio identification. IEEE Communications Magazine 56(9):146–152.

doi:10.1109/MCOM.2018.1800153

80. Merchant, K., Revay, S., Stantchev, G. & Nousain, B. (2018). Deep learning for RF device fingerprinting in cognitive communication networks. IEEE Journal of Selected Topics in Signal Processing 12(1):160–167. doi:10.1109/JSTSP.2018.2796446

81. Kaushal, H. & Kaddoum, G. (2017). Optical communication in space: challenges and mitigation techniques. IEEE Communications Surveys & Tutorials 19(1):57–96. doi:10.1109/COMST.2016.2603518 ARXIV PREPRINT ↗

82. Klein, B. J. & Degnan, J. J. (1974). Optical antenna gain. 1: Transmitting antennas. Applied Optics 13(9):2134–2141. doi:10.1364/AO.13.002134 Corroborated by: Safi, H., Wang, Z., Mast, S., Haas, H. & Tavakkolnia, I. (2026). Analytical channel modeling and stability aware optimization of optical inter-satellite links. arXiv:2609.17431 ARXIV ↗ .

83. Papoulis, A. & Pillai, S. U. (2002). Probability, Random Variables and Stochastic Processes, 4th ed. New York: McGraw-Hill.

84. Benford, J., Swegle, J. A. & Schamiloglu, E. (2016). High Power Microwaves, 3rd ed. Boca Raton: CRC Press.

85. Zervas, M. N. & Codemard, C. A. (2014). High power fiber lasers: a review. IEEE Journal of Selected Topics in Quantum Electronics 20(5):219–241 (article 0904123). doi:10.1109/JSTQE.2014.2321279 Corroborated by: Hecht, J. (13 Apr 2016). Photonic Frontiers: High-efficiency optical pumping. Laser Focus World 52(4) LASERFOCUSWORLD.COM ↗ .

86. Lockheed Martin (28 Jan 2014). Lockheed Martin Demonstrates Weapons-Grade High Power Fiber Laser [press release]. Bothell, WA. NEWS.LOCKHEEDMARTIN.COM ↗

87. Hecht, J. (13 Apr 2016). Photonic Frontiers: High-efficiency optical pumping: 'Going green' cranks up the laser power. Laser Focus World 52(4). LASERFOCUSWORLD.COM ↗

88. Lockheed Martin (18 Aug 2022). Lockheed Martin Delivers Integrated Multi-Mission Laser Weapon System to the Navy [press release on HELIOS, 60+ kW class]. Related: Lockheed Martin (28 Jul 2023), Lockheed Martin to Scale Its Highest Powered Laser to 500 Kilowatts Power Level (OUSD(R&E) High Energy Laser Scaling Initiative, HELSI). NEWS.LOCKHEEDMARTIN.COM ↗

89. Air Force Research Laboratory (30 Jul 2021). AFRL's drone killer, THOR will welcome new drone 'hammer' [news release on THOR and the Mjolnir follow-on]. CHAMP: Boeing/AFRL flight test, Utah Test and Training Range, 16 Oct 2012. AFRESEARCHLAB.COM ↗

90. Missile Defense Agency (Jan 2024). Ground-based Midcourse Defense [fact sheet, 24-MDA-11677]. MDA.MIL PDF ↗

91. L3Harris Technologies (Dec 2025). L3Harris Delivers First Meadowlands Production Unit to US Space Force [news release; Meadowlands is the upgraded Counter Communications System].

L3HARRIS.COM ↗

92. Albon, C. (15 Apr 2025). Space Force 'Meadowlands' jammer ready for formal testing. Defense News. DEFENSENEWS.COM ↗

93. NASA (2023). DSOC (Deep Space Optical Communications) Technology Demonstration [fact sheet, dated 15 Jun 2023]. NASA/JPL-Caltech. NASA.GOV PDF ↗

94. Speed, R. (30 Sep 2025). NASA's deep-space laser comms demo has left the chat. The Register. THEREGISTER.COM ↗

POWER AND HEAT

§6

95. Henninger, J. H. (1984). Solar Absorptance and Thermal Emittance of Some Common Spacecraft Thermal-Control Coatings. NASA Reference Publication 1121, NASA Goddard Space Flight Center. NASA NTRS PDF ↗

96. Mason, L. S. (2003). A Power Conversion Concept for the Jupiter Icy Moons Orbiter. NASA/TM-2003-212596 (AIAA 2003-6007, 1st International Energy Conversion Engineering Conference), NASA Glenn Research Center. NASA NTRS PDF ↗

97. Mason, L. S. (2004). Power-Conversion Concept Designed for the Jupiter Icy Moons Orbiter. In Research and Technology 2003, NASA Glenn Research Center. NTRS 20050192432. NASA NTRS PDF ↗

98. Siamidis, J., Mason, L., Beach, D. & Yuko, J. (2005). Heat Rejection Concepts for Brayton Power Conversion Systems. NASA/TM-2005-213337 (AIAA 2004-5654, 2nd International Energy Conversion Engineering Conference). NASA NTRS PDF ↗

99. Poston, D. I., Gibson, M. A., Sanchez, R. G. & McClure, P. R. (2020). Results of the KRUSTY Nuclear System Test. Nuclear Technology 206(sup1):S89-S117. doi:10.1080/00295450.2020.1730673 OSTI PDF ↗

100. Choi, M. K. (2012). Phase Change Material for Temperature Control of Loop Heat Pipe Compensation Chamber. 10th International Energy Conversion Engineering Conference (AIAA), NASA GSFC. NTRS 20120015405. NASA NTRS PDF ↗

101. Choi, M. K. (2018). Thermal Assessment of Paraffin Phase Change Material Mini-Packs on IceCube 3U CubeSat in Flight. 2018 AIAA Propulsion and Energy Forum, NASA GSFC. NTRS 20180004470. NASA NTRS PDF ↗

102. Leimkuehler, T. O., Stephan, R. A. & Hawkins-Reynolds, E. (2011). Testing and Failure Mechanisms of Ice Phase Change Material Heat Exchangers. 41st International Conference on Environmental Systems (AIAA), NASA JSC. NTRS 20110008723. NASA NTRS PDF ↗

103. Gilmore, D. G. (ed.) (2002). Spacecraft Thermal Control Handbook, Vol. 1: Fundamental Technologies, 2nd ed. The Aerospace Press / AIAA, El Segundo, CA. Corroborated by: Gaite, J. & Fernández-Rico, G. (2012). Linear approach to the orbiting spacecraft thermal problem. Journal of Thermophysics and Heat Transfer 26:511-522. arXiv:1202.4372 ARXIV ↗ .

104. Incropera, F. P., DeWitt, D. P., Bergman, T. L. & Lavine, A. S. (2007). Fundamentals of Heat and Mass Transfer, 6th ed. Wiley. Corroborated by: Çengel, Y. A. & Ghajar, A. J. Heat and Mass Transfer: Fundamentals and Applications, Appendix 1, Table A-3 'Properties of solid metals' (free appendix PDF from McGraw-Hill) HIGHERED.MHEDUCATION.COM PDF ↗ .

105. Chase, M. W., Jr. (1998). NIST-JANAF Thermochemical Tables, 4th ed., J. Phys. Chem. Ref. Data Monograph 9; as tabulated in the NIST Chemistry WebBook, SRD 69: Aluminum, solid-phase Shomate equation, 298–933 K (Cp = 24.21 J/mol·K at 298.15 K, 897 J/kg·K). NIST WEBBOOK ↗

106. Cox, A. N. (ed.) (2000). Allen's Astrophysical Quantities, 4th ed. AIP Press / Springer, New York. Corroborated by: Tripathi, A. K., Chaubey, S. & Singh, A. K. (2020). Study of Limb Darkening Effect and Rotation Period of Sun by using Solar Telescope. Journal of Scientific Research (Banaras Hindu University) 64(1). doi:10.37398/JSR.2020.640132 BHU.AC.IN PDF ↗ .

107. Hanel, R. A., Conrath, B. J., Herath, L. W., Kunde, V. G. & Pirraglia, J. A. (1981). Albedo, internal heat, and energy balance of Jupiter: Preliminary results of the Voyager infrared investigation. Journal of Geophysical Research 86(A10):8705-8712. doi:10.1029/JA086iA10p08705 NASA NTRS PDF ↗

108. Li, L., Jiang, X., West, R. A., Gierasch, P. J., Perez-Hoyos, S., Sanchez-Lavega, A., Fletcher, L. N., Fortney, J. J. et al. (2018). Less absorbed solar energy and more internal heat for Jupiter. Nature Communications 9:3709. doi:10.1038/s41467-018-06107-2 NATURE (OPEN) ↗

109. Kopp, G. & Lean, J. L. (2011). A new, lower value of total solar irradiance: Evidence and climate significance. Geophysical Research Letters 38:L01706. doi:10.1029/2010GL045777 AGU (OPEN) ↗

110. Edwards, D. (2012). An Overview of the Jupiter Icy Moons Orbiter (JIMO) Mission, Environments, and Materials Challenges. NASA MSFC presentation, 12th International Symposium on Materials in the Space Environment. NTRS 20120016895. [Programme: NASA Project Prometheus, JIMO, 2003-2005.] NASA NTRS PDF ↗

INFRARED AND OPTICAL SENSING

§6

111. Planck, M. (1901). Ueber das Gesetz der Energieverteilung im Normalspectrum. Annalen der Physik 309(3):553-563 (4. Folge, Bd. 4). doi:10.1002/andp.19013090310 WIKISOURCE ↗

112. Widger, W. K. & Woodall, M. P. (1976). Integration of the Planck blackbody radiation function. Bulletin of the American Meteorological Society 57(10):1217-1219. doi:10.1175/1520-0477(1976)057<1217:IOTPBR>2.0.CO;2 AMS (OPEN) ↗ Corroborated by: Lewis, W. & McClarren, R. G.

(2025). Fast, Accurate Numerical Evaluation of Incomplete Planck Integrals. arXiv:2503.08892 (University of Notre Dame) ARXIV ↗ .

113. Hudson, R. D. (1969). Infrared System Engineering. Wiley, New York. Corroborated by: OpenStax, University Physics Volume 2, §1.6 Mechanisms of Heat Transfer (Rice University, CC BY) OPENSTAX ↗ .

114. Hecht, E. (2017). Optics, 5th ed. Pearson. Corroborated by: OpenStax, University Physics Volume 3, §4.5 Circular Apertures and Resolution, Eq. (4.5) OPENSTAX ↗ ; Barbastathis, G. MIT OCW 2.71 Optics (Spring 2009), Lecture 17: Fraunhofer diffraction; Fourier transforms and theorems MIT OCW ↗ .

115. Mainzer, A. K., Masiero, J. R., Abell, P. A., Bauer, J. M., Bottke, W. et al. (2023). The Near-Earth Object Surveyor Mission. Planetary Science Journal 4(12):224. doi:10.3847/PSJ/ad0468 IOP (OPEN) ↗

116. NASA Jet Propulsion Laboratory. Near-Earth Object Surveyor (mission page). Accessed 2026. JPL.NASA.GOV ↗

117. Matsumoto, T., Tsumura, K., Matsuoka, Y. & Pyo, J. (2018). Zodiacal light beyond Earth orbit observed with Pioneer 10. Astronomical Journal 156(3):86. doi:10.3847/1538-3881/aad0f0 ARXIV ↗

118. Leinert, Ch., Bowyer, S., Haikala, L. K., Hanner, M. S., Hauser, M. G., Levasseur-Regourd, A.-Ch., Mann, I., Mattila, K. et al. (1998). The 1997 reference of diffuse night sky brightness. Astronomy and Astrophysics Supplement Series 127:1-99. doi:10.1051/aas:1998105 AAS.AANDA.ORG PDF ↗

119. Stokes, G. H., Weber, R., Shelly, F. C., Beatty, D. E., Viggh, H. E. M., Rork, E. W. & Hays, B. (1996). Air Force Planetary Defense System: Initial Field Test Results. In Space 96: Proceedings of the Fifth International Conference on Space, Engineering, Construction, and Operations in Space V (ASCE), Albuquerque, 1-6 June 1996, pp. 46-53. doi:10.1061/40177(207)7 Corroborated by: Stokes, G. H., Evans, J. B., Viggh, H. E. M., Shelly, F. C. & Pearce, E. C. (1998). The Lincoln Near-Earth Asteroid Research (LINEAR) Program. Lincoln Laboratory Journal 11(1):27-40 MIT LL PDF ↗ .

120. U.S. Space Force. Ground-Based Electro-Optical Deep Space Surveillance (GEODSS) fact sheet (sites: Socorro NM, Maui HI, Diego Garcia). SPACEFORCE.MIL ↗

121. Johnson, J. (1958). Analysis of image forming systems. In Proceedings of the Image Intensifier Symposium, 6-7 October 1958, U.S. Army Engineer Research and Development Laboratories, Fort Belvoir, VA, pp. 244-273 (DTIC AD220160). Corroborated by: Sjaardema, T. A., Smith, C. S. & Birch, G. C. (2015). History and Evolution of the Johnson Criteria. Sandia National Laboratories, SAND2015-6368. OSTI 1222446 OSTI PDF ↗ .

122. Madhusudhan, N. & Burrows, A. (2012). Analytic models for albedos, phase curves, and polarization of reflected light from exoplanets. Astrophysical Journal 747(1):25. doi:10.1088/0004-637X/747/1/25 ARXIV ↗

123. Willmer, C. N. A. (2018). The absolute magnitude of the Sun in several filters. Astrophysical Journal Supplement Series 236(2):47. doi:10.3847/1538-4365/aabfdf ARXIV ↗

124. Torres, G. (2010). On the use of empirical bolometric corrections for stars. Astronomical Journal 140(5):1158–1162. doi:10.1088/0004-6256/140/5/1158 ARXIV ↗

TRACKING

§7

125. Julier, S. J. & Uhlmann, J. K. (2004). Unscented filtering and nonlinear estimation. Proceedings of the IEEE 92(3):401–422. doi:10.1109/JPROC.2003.823141 Corroborated by: filterpy 1.4.5 documentation, JulierSigmaPoints (R. Labbe) FILTERPY.READTHEDOCS.IO ↗ .

126. Bar-Shalom, Y., Li, X. R. & Kirubarajan, T. (2001). Estimation with Applications to Tracking and Navigation. New York: Wiley. Corroborated by: Labbe, R. R. Kalman and Bayesian Filters in Python (open textbook, CC-BY 4.0) GITHUB ↗ ; Labbe, R. R. Kalman and Bayesian Filters in Python, ch. 14 'Adaptive Filtering' (open textbook) GITHUB ↗ .

127. Lindgren, A. G. & Gong, K. F. (1978). Position and velocity estimation via bearing observations. IEEE Transactions on Aerospace and Electronic Systems AES-14(4):564–577. doi:10.1109/TAES.1978.308681 Corroborated by: Bu, S., Meng, A. & Zhou, G. (2021). A New Pseudolinear Filter for Bearings-Only Tracking without Requirement of Bias Compensation. Sensors 21(16):5444 PMC (OPEN) ↗ .

128. Aidala, V. J. & Nardone, S. C. (1982). Biased estimation properties of the pseudolinear tracking filter. IEEE Transactions on Aerospace and Electronic Systems AES-18(4):432–441. doi:10.1109/TAES.1982.309250 Corroborated by: Bu, S., Meng, A. & Zhou, G. (2021). Sensors 21(16):5444 PMC (OPEN) ↗ .

129. Woffinden, D. C. & Geller, D. K. (2009). Observability criteria for angles-only navigation. IEEE Transactions on Aerospace and Electronic Systems 45(3):1194–1208. doi:10.1109/TAES.2009.5259193

130. Blackman, S. & Popoli, R. (1999). Design and Analysis of Modern Tracking Systems. Norwood, MA: Artech House. Corroborated by: MathWorks. trackHistoryLogic (Sensor Fusion and Tracking Toolbox documentation), citing Blackman & Popoli 1999 MATHWORKS.COM ↗ .

DEBRIS AND BREAKUP

§5

131. Johnson, N. L., Krisko, P. H., Liou, J.-C. & Anz-Meador, P. D. (2001). NASA's new breakup model of EVOLVE 4.0. Advances in Space Research 28(9):1377–1384. doi:10.1016/S0273-1177(01)00423-9 Corroborated by: Frey, S. & Colombo, C. (2021). Transformation of satellite breakup distribution for probabilistic orbital collision hazard analysis. JGCD 44(1):88–105 (PoliMi IRIS open-access copy) RE.PUBLIC.POLIMI.IT PDF ↗ ; Krisko, P. H. (2011). Proper implementation of the 1998 NASA breakup

model. ODQN 15(4):4–5 NASA ODPO PDF ↗ ; Panarotto, S. (2024, a.y. 2023/24). Analisi del delta V di detriti spaziali generati a seguito di eventi di frammentazione in orbita. MSc thesis, Univ. Padova THESIS.UNIPD.IT PDF ↗ .

132. Krisko, P. H. (2011). Proper implementation of the 1998 NASA breakup model. Orbital Debris Quarterly News 15(4):4–5. NASA ODPO PDF ↗

133. Joubert, W. & Tingay, S. (2020). Simulations of orbital debris clouds due to breakup events and their characterisation using the Murchison Widefield Array radio telescope. Experimental Astronomy 51(1):61–75 (issue dated 2021). doi:10.1007/s10686-020-09684-7; arXiv:2008.03657 ARXIV ↗

134. Thiele, S. & Boley, A. C. (2022). Investigating the risks of debris-generating ASAT tests in the presence of megaconstellations. The Journal of the Astronautical Sciences 69(6):1797–1820. doi:10.1007/s40295-022-00356-6; arXiv:2111.12196 ARXIV ↗

135. Frey, S. & Colombo, C. (2021). Transformation of satellite breakup distribution for probabilistic orbital collision hazard analysis. Journal of Guidance, Control, and Dynamics 44(1):88–105. doi:10.2514/1.G004939. Appendix B: the NASA standard breakup model as implemented. RE.PUBLIC.POLIMI.IT PDF ↗

136. Panarotto, S. (2024; academic year 2023/24). Analisi del delta V di detriti spaziali generati a seguito di eventi di frammentazione in orbita [Analysis of the delta-V of space debris generated by in-orbit fragmentation events]. MSc thesis (Laurea Magistrale, Ingegneria Aerospaziale), Università degli Studi di Padova; supervisor L. Olivieri. THESIS.UNIPD.IT PDF ↗

137. NASA Orbital Debris Program Office (2007). Chinese anti-satellite test creates most severe orbital debris cloud in history. Orbital Debris Quarterly News 11(2):2–3. And: (2022). The intentional destruction of Cosmos 1408. Orbital Debris Quarterly News 26(1):1–4. NASA ODPO PDF ↗

138. Anz-Meador, P. D., Opiela, J. N., Shoots, D. & Liou, J.-C. (2018). History of On-orbit Satellite Fragmentations, 15th ed. NASA/TM-2018-220037, NASA JSC Orbital Debris Program Office. NASA NTRS PDF ↗

DOCTRINE §8

139. Joint Chiefs of Staff (2020). JP 3-85, Joint Electromagnetic Spectrum Operations, 22 May 2020. FAS PDF ↗

140. Joint Chiefs of Staff (2018, incorporating Change 1, 26 Oct 2020). JP 3-14, Space Operations, 10 April 2018. FAS PDF ↗

141. Joint Chiefs of Staff (2018). JP 3-60, Joint Targeting, 28 September 2018. ESD.WHS.MIL PDF ↗

142. U.S. Air Force, LeMay Center (2026). AFDP 3-60, Targeting, 1 May 2026. DOCTRINE.AF.MIL PDF ↗

143. U.S. Space Force (2025). Space Warfighting: A Framework for Planners. March 2025 (released April 2025). CSPS.AEROSPACE.ORG PDF ↗

144. U.S. Space Force (2025). Space Force Doctrine Document 1 (SFDD-1), The Space Force, signed 3 April 2025. SPACEFORCE.MIL PDF ↗

145. Department of Defense (2014). MIL-STD-2525D, Department of Defense Interface Standard: Joint Military Symbology, 10 June 2014. JCS.MIL PDF ↗ Corroborated by: milsymbol (spatialillusions), MIL-STD-2525D implementation test page reproducing the standard's tables CDN.JSDELIVR.NET ↗ .

THE SETTING AND THE SCENARIO §9

146. U.S. Space Force, Combat Forces Command (formerly Space Operations Command). Fact sheet: Mission Delta 2 - Space Domain Awareness (companion fact sheets: Delta 3 - Space Electromagnetic Warfare; Delta 9 - Orbital Warfare). USSF-CFC.SPACEFORCE.MIL ↗

147. Combined Space Operations (CSpO) Initiative (2022). Combined Space Operations Vision 2031. Released February 2022. DEFENCE.GOVT.NZ PDF ↗

148. NATO. NATO's approach to space (official topic page; documents the December 2019 London Declaration recognising space as an operational domain and the October 2020 decision to establish a NATO Space Operations Centre at Allied Air Command, Ramstein). NATO.INT ↗

149. UK Ministry of Defence (2021). UK Space Command (GOV.UK guidance page, published 1 April 2021; withdrawn 25 June 2026). GOV.UK ↗

150. U.S. Space Force. Fact sheet: Geosynchronous Space Situational Awareness Program (GSSAP) (current as of Oct 2020). SPACEFORCE.MIL ↗

151. National Reconnaissance Office. SILENTBARKER/NROL-107 launch page (launched 10 September 2023; joint NRO-U.S. Space Force space domain awareness mission). NRO.GOV ↗

152. U.S. Space Force / SAF Public Affairs (2 December 2023). US, UK, Australia announce trilateral Deep Space Advanced Radar Capability initiative. SPACEFORCE.MIL ↗

153. Defense Intelligence Agency (2022). Challenges to Security in Space 2022 (follow-up to the February 2019 edition). DIA.MIL PDF ↗ Corroborated by: Joint Chiefs of Staff news (11 Feb 2019), 'Defense Intelligence Agency releases report on challenges to U.S. security in space' JCS.MIL ↗ ; Weeden, B. & Samson, V. (eds.) (2023). Global Counterspace Capabilities, Secure World Foundation SWF PDF ↗ .

154. Strout, N., Defense News (23 July 2020). Russia conducted anti-satellite test in space, says US Space Command. Reports the USSPACECOM statement that Cosmos 2543 released an object in a non-destructive on-orbit ASAT test on 15 July 2020. DEFENSENEWS.COM ↗

155. Swope, C., Bingen, K. A., Young, M., Chang, M., Songer, S. & Tammelleo, J. (2024). Space Threat Assessment 2024. CSIS Aerospace Security Project, April 2024. AEROSPACE.CSIS.ORG PDF ↗

156. Weeden, B. & Samson, V. (eds.) (2023). Global Counterspace Capabilities: An Open Source Assessment. Secure World Foundation. Co-orbital inspection, including Luch/Olymp-K at GEO from 2014, Cosmos 2542/2543 shadowing USA 245 (2019–2020) and Shijian-21 towing Compass-G2 (2022). SWF PDF ↗

157. Xinhua, via China Aerospace Science and Technology Corporation (20 March 2024). China launches new relay satellite for Earth-Moon communications (Queqiao-2). The original Queqiao (2018) operates in an Earth-Moon L2 halo orbit. ENGLISH.SPACECHINA.COM ↗

158. Hitchens, T., Breaking Defense (19 October 2026). Russian satellite stalked ICEYE spacecraft in potentially dangerous on-orbit maneuvers. BREAKINGDEFENSE.COM ↗

159. Trevithick, J. & Altman, H., The War Zone (19 October 2026). Russian Satellite's Unprecedented Shadowing Of A Very Particular Radar Imaging Satellite Is A Big Deal. TWZ.COM ↗

160. ESA Earth Online. ICEYE (mission description: X-band SAR constellation of sub-100 kg satellites). EARTH.ESA.INT ↗

161. NASA/JPL (16 June 2016). NASA's Juno Spacecraft to Risk Jupiter's Fireworks for Science. News release. JPL.NASA.GOV ↗

162. Harwood, W., CBS News (2 Jul 2010). Progress docking aborted: Progress M-06M lost its telemetry link on final approach to the ISS and flew past. CBSNEWS.COM ↗

UNITS AND CONSTANTS

163. BIPM (2019). The International System of Units (SI), 9th edition (SI Brochure). BIPM.ORG PDF ↗

164. Tiesinga, E., Mohr, P. J., Newell, D. B. & Taylor, B. N. (2021). CODATA recommended values of the fundamental physical constants: 2018. Rev. Mod. Phys. 93, 025010. PHYSICS.NIST.GOV PDF ↗

165. Thompson, A. & Taylor, B. N. (2008). Guide for the Use of the International System of Units (SI). NIST Special Publication 811, 2008 edition. NVLPUBS.NIST.GOV PDF ↗

CLOSE PASS AT THE EARTH

§2, §4.5, §9

166. CelesTrak. General perturbations (GP) element sets, ICEYE-X36 (NORAD 59103), epoch 26 October 2026 21:06 UTC. CELESTRAK.ORG ↗

167. Vallado, D. A., Crawford, P., Hujsak, R. & Kelso, T. S. (2006). Revisiting Spacetrack Report #3. AIAA/AAS Astrodynamics Specialist Conference, AIAA 2006-6753. Code: CelesTrak, SGP4 software.

CELESTRAK.ORG ↗

168. KeepTrack. Cosmos 2612 / ICEYE-X36 rendezvous, an analysis from public element sets (19 October 2026, updated 23 October). KEEPTRACK.SPACE ↗

169. Krebs, G. D. Gunter's Space Page: ICEYE (spacecraft entry).

170. McDowell, J. C. General Catalog of Artificial Space Objects (GCAT), release 1.8.

171. Nicolls, M. J., Vittaldev, V., Ceperley, D., Creus-Costa, J., Foster, C., Griffith, N., Lu, E., Mason, J., Park, I., Rosner, C. & Stevenson, M. (2017). Conjunction Assessment for Commercial Satellite Constellations Using Commercial Radar Data Sources. Advanced Maui Optical and Space Surveillance Technologies Conference (AMOS).

172. Stevenson, M., Nicolls, M. J., Park, I. & Rosner, C. (2020). Measurements of the Kiwi Space Radar. Advanced Maui Optical and Space Surveillance Technologies Conference (AMOS).

173. Federal Communications Commission. Experimental radio service licence WO2XME (LeoLabs, Arizona). FCC Office of Engineering and Technology, experimental licensing system.

© 2026 Kevin Williamson. All rights reserved. Planetary data from NASA and JPL, used as published; NASA and JPL have not reviewed or endorsed this game. Earth imagery from NASA Earth Observatory (Blue Marble). CLOSE PASS draws on a real event, real satellites and real radar sites from public reporting and public tracking data; WATCHMAN-1 and the scenario's events after its start are notional.